

1                   **Subcytoplasmic location of translation controls protein output**

2  
3   Ellen L. Horste<sup>1,2</sup>, Mervin M. Fansler<sup>2,3</sup>, Ting Cai<sup>2</sup>, Xiuzhen Chen<sup>2</sup>, Sibylle Mitschka<sup>2</sup>, Gang  
4   Zhen<sup>2</sup>, Flora C. Y. Lee<sup>4,5</sup>, Jernej Ule<sup>4,5</sup>, and Christine Mayr<sup>1,2,3†</sup>

5   <sup>1</sup>Gerstner Sloan Kettering Graduate School of Biomedical Sciences, New York, NY 10065, USA

6   <sup>2</sup>Cancer Biology and Genetics Program, Sloan Kettering Institute, New York, NY 10065, USA

7   <sup>3</sup>Tri-Institutional Training Program in Computational Biology and Medicine, Weill-Cornell

8   Graduate College, New York, NY 10021, USA

9   <sup>4</sup>UK Dementia Research Institute, King's College London, London, SE5 9NU, UK

10   <sup>5</sup>The Francis Crick Institute, 1 Midland Road, London NW1 1AT, UK

11   <sup>†</sup>Correspondence: [mayrc@mskcc.org](mailto:mayrc@mskcc.org)

12  
13   **Summary**

14   The cytoplasm is highly compartmentalized, but the extent and consequences of  
15   subcytoplasmic mRNA localization in non-polarized cells are largely unknown. We determined  
16   mRNA enrichment in TIS granules (TGs) and the rough endoplasmic reticulum (ER) through  
17   particle sorting and isolated cytosolic mRNAs by digitonin extraction. When focusing on non-  
18   membrane protein-encoding mRNAs, we observed that 52% have a biased transcript  
19   distribution across these compartments. Compartment enrichment is determined by a  
20   combinatorial code based on mRNA length, exon length, and 3'UTR-bound RNA-binding  
21   proteins. Compartment-biased mRNAs differ in the functional classes of their encoded proteins:  
22   TG-enriched mRNAs encode low-abundance proteins with strong enrichment of transcription  
23   factors, whereas ER-enriched mRNAs encode large and highly expressed proteins.  
24   Compartment localization is an important determinant of mRNA and protein abundance, which  
25   is supported by reporter experiments showing that redirecting cytosolic mRNAs to the ER  
26   increases their protein expression. In summary, the cytoplasm is functionally compartmentalized  
27   by local translation environments.

28  
29   **Keywords**

30   Cytoplasmic organization; spatial regulation of protein synthesis; cytoplasmic compartments;  
31   condensates; TGs; mRNA localization; gene expression regulation; functional  
32   compartmentalization; translation environment; translation regulation; compartment-dependent  
33   mRNA abundance regulation; rough endoplasmic reticulum membrane; gene architecture;  
34   mRNA length; exon length; 3'UTR; RNA-binding proteins; CLIP analysis; TIS11B; TIAL1;  
35   LARP4B; TIS11B knockout

36  
37   **Introduction**

38   In polarized cells such as neurons, intestinal epithelial cells, or cells of the early fly embryo, the  
39   majority of mRNAs have a distinct spatial localization pattern.<sup>1-5</sup> mRNA localization enables the  
40   local control of protein production and activity.<sup>6-8</sup> In non-polarized cells, mRNA localization has  
41   primarily been studied for membrane proteins, which mostly localize to the endoplasmic  
42   reticulum (ER) or to mitochondria.<sup>9-12</sup> Whereas the rough ER is established as major site of  
43   local protein synthesis for membrane and secretory proteins,<sup>9,10,13</sup> the cytoplasm is  
44   compartmentalized by additional membrane-bound and membraneless organelles.<sup>14-17</sup> Some of  
45   these compartments may enable the generation of unique biochemical translation

46 environments, which have been suggested to be crucial for protein interaction partner selection  
47 during protein synthesis,<sup>16,18-20</sup> but it is currently largely unknown if the location of protein  
48 synthesis also matters for protein output.

49 TIS granules (TGs) represent one such unique translation compartment, which promotes the co-  
50 translational formation of protein complexes.<sup>16,19</sup> TGs are formed by the RNA-binding protein  
51 (RBP) TIS11B together with its bound mRNAs.<sup>16,21</sup> *TIS11B* mRNA is ubiquitously expressed,<sup>22</sup>  
52 suggesting that TGs are widespread. TGs are present under steady-state cultivation conditions  
53 and form a network-like structure that is intertwined with the rough ER.<sup>16,21</sup> To investigate the  
54 broader biological significance of TGs, we set out to determine the mRNAs enriched in TGs, the  
55 neighboring rough ER, and the surrounding cytosol.

56 As TIS11B protein is present in cells in two states (Fig. 1A), (i) as soluble protein in the cytosol,  
57 and (ii) as phase-separated TG network,<sup>16,21</sup> we decided to use fluorescent particle sorting<sup>23</sup> to  
58 identify mRNAs enriched in TGs. We also applied fluorescent particle sorting to isolate ER-  
59 enriched mRNAs and extracted cytosolic mRNAs using digitonin. We focused our analysis on  
60 mRNAs that encode non-membrane proteins and found more than 3600 mRNAs to be  
61 consistently enriched in one of the three compartments. mRNAs enriched in each compartment  
62 share similar mRNA architectures which differ substantially between compartments.  
63 Compartment-enriched mRNAs also differed significantly in production and degradation rates as  
64 well as in the functional classes and expression levels of their encoded proteins. TIS11B  
65 knockout (KO) and reporter experiments support a model by which a combinatorial code  
66 consisting of mRNA architecture features together with 3'UTR-bound RBPs, including TIS11B,  
67 TIA1/L1, and LARP4B, largely determines the compartment-biased mRNA localization pattern.  
68 Intriguingly, we observed that redirecting cytosolic mRNAs to the ER controls protein  
69 expression, which indicates that protein abundance regulation is spatially regulated in the  
70 cytoplasm.

71

## 72 Results

### 73 Approach to determine subcytoplasmic mRNA localization

74 We set out to identify mRNAs that are localized in non-polarized human HEK293T cells under  
75 steady-state cultivation conditions. We focused on three major unenclosed cytoplasmic  
76 compartments—TGs, a condensate network formed by the RBP TIS11B, the cytosolic surface  
77 of the ER, and the soluble part of the cytoplasm known as the cytosol (Fig. 1B). For simplicity,  
78 we consider here the sum of the three compartments as the universe of cytoplasmic mRNAs.

79 To identify TG-enriched (TG+) and ER-enriched (ER+) mRNAs, we performed fluorescent  
80 particle sorting followed by RNA-seq. After co-transfected cells with mCherry-TIS11B and GFP-  
81 SEC61B to label TGs and rough ER, respectively, we used mechanical lysis and differential  
82 centrifugation to isolate the cytoplasmic membrane fraction, followed by flow cytometry-based  
83 sorting of fluorescent particles (Fig. S1A, S1B). DAPI staining allowed us to identify and discard  
84 TG and ER particles that were still associated with nuclei. We used confocal microscopy to  
85 assess the purity of the particles. While ER particles generally did not contain mCherry-TIS11B,  
86 most of the TG particles contained GFP-SEC61B, consistent with the intimate association of TG  
87 and ER inside cells (Fig. 1C). Using western blot analysis, we observed that both particles  
88 contain similar amounts of ER proteins such as Calnexin and GFP-SEC61B, but TG particles  
89 contain 13-fold more mCherry-TIS11B than ER particles (Fig. S1C-E). As TG are defined by the  
90 presence of TIS11B,<sup>16</sup> we reasoned that the strong overrepresentation of TIS11B in TG  
91 particles would allow us to identify relative enrichments of mRNAs between the compartments.

92 For subsequent RNA-seq experiments, we sorted TG particles from the TIS11B+SEC61B+  
93 population and we sorted ER particles from the TIS11B-SEC61B+ population (Fig. S1B).  
94 To isolate cytosolic mRNAs, we used digitonin extraction.<sup>24</sup> The extracted cytosol was not  
95 contaminated by nuclei or the ER, but it contained cytosolic proteins, including GAPDH which  
96 was used as a positive control (Fig. S1C). It also contained TIS11B, which was expected since  
97 soluble TIS11B is known to be present in the cytosol. We performed RNA-seq to determine the  
98 mRNA composition in the three fractions and focused our analysis on protein-coding mRNAs.  
99 The biological replicate samples of each compartment correlated well (Fig. S1F).

100

### 101 **mRNAs that encode membrane or secretory proteins largely localize to the ER membrane**

102 We set out to investigate if the relative mRNA transcript distribution differs across the three  
103 compartments. For each gene, we determined a compartment-specific localization score. This  
104 score is calculated using the RPKM value obtained in each of the three compartments  
105 respectively and dividing it by the sum of the RPKM values in all three compartments. Thus,  
106 each gene is assigned three localization scores that correspond to the fraction of its transcripts  
107 localizing to each of the three compartments: TGs, the ER, and the cytosol.

108 It is accepted that most mRNAs that encode membrane or secretory proteins are translated on  
109 the ER.<sup>10,11,13</sup> To account for the difference in distribution, we plotted the localization scores of  
110 mRNAs that encode membrane/secretory proteins separately from the rest of the mRNAs that  
111 encode non-membrane proteins (Fig. S1G). In line with previous analyses, we find preferential  
112 partitioning of mRNAs encoding membrane/secretory proteins in the ER samples (Fig. S1G).  
113<sup>10,11,13</sup> To examine if our compartment isolation method is valid, we compared it with datasets  
114 derived from three alternative isolation methods.<sup>9,11,13</sup> In our analysis, we consider 69% ( $N =$   
115 1,476) of membrane/secretory proteins to be enriched on the ER (Fig. S1H, Table S1). When  
116 comparing our results with mRNAs identified by biochemical fractionation, MERFISH or APEX-  
117 seq, we detected between 80-90% overlap and our data showed a quantitative relationship with  
118 data obtained by APEX-seq (Fig. S1I, S1J).<sup>9,11,13</sup> These results strongly support the validity of  
119 our purification strategy for mRNAs that encode membrane/secretory proteins.

120

### 121 **Half of mRNAs that encode non-membrane proteins have a biased transcript distribution 122 in the cytoplasm**

123 It was unclear whether non-membrane protein encoding mRNAs are biased in their localization.  
124 Not surprisingly, we found that these mRNAs have more evenly distributed localization scores  
125 across the three compartments (Fig. S1G). To faithfully compare absolute differences in mRNA  
126 distribution across the three compartments, the relative size of each compartment needs to be  
127 considered. However, this parameter is currently unknown. Therefore, instead, we calculated  
128 the relative enrichment of mRNAs within each compartment. We considered an mRNA  
129 compartment-enriched, if its mean localization score across biological replicates was at least  
130 1.25-fold higher than the median localization score of the compartment samples (Fig. 1D-F).  
131 Based on this criterion, we identified 1246 TG+ mRNAs, 919 ER+ mRNAs, and 1481 mRNAs  
132 enriched in the cytosol (CY+), which were non-overlapping (Fig. 1D-F, Table S1). The remaining  
133 3369 mRNAs were not enriched in a single compartment and were considered to have an  
134 unbiased localization pattern (Fig. 1D-F, Fig. S1K). Fig. 1D-F illustrate that the distribution of  
135 TG+, ER+, or CY+ localization scores are significantly different from the localization scores of  
136 mRNAs with unbiased localization patterns. Since localization scores across the three  
137 compartments sum to 1, an mRNA enriched in one compartment is relatively de-enriched in the  
138 other two (Fig. S1L). Based on this strategy, 52% of mRNAs that encode non-membrane

139 proteins are significantly enriched in one of the three subcytoplasmic compartments in steady-  
140 state conditions.

141 As a recent study also analyzed the relative distribution of mRNA transcripts across subcellular  
142 compartments, we compared our compartment enrichment data with their results.<sup>25</sup> Although  
143 their dataset was generated by density gradient centrifugation in a different cell line, the two  
144 compartment enrichment datasets strongly agree in a qualitative and quantitative manner (Fig.  
145 S1M), suggesting that our isolation method as well as our strategy to define compartment-  
146 enriched mRNAs are valid. As non-membrane protein encoding mRNAs with biased transcript  
147 distributions in the cytoplasm have not been systematically characterized, we focused all  
148 subsequent analyses on mRNAs that encode non-membrane proteins.

149

## 150 **Validation of compartment-enriched mRNAs by single-molecule RNA-FISH**

151 We further validated the mRNAs designated as compartment-enriched by performing single-  
152 molecule (sm) RNA-FISH on endogenous mRNAs (Table S2).<sup>26</sup> To distinguish between TG+  
153 and ER+ mRNAs, we performed smRNA-FISH together with co-transfection of BFP-TIS11B and  
154 GFP-SEC61B to simultaneously visualize mRNA puncta, TGs, and the rough ER (Fig. 1G, 1H,  
155 Fig. S2A-G). Here, we considered an mRNA to have an unbiased localization pattern if its  
156 transcript distribution correlated with compartment size. As proxy for relative compartment size,  
157 we used the areas of the maximum projection of the fluorescent signals for each compartment  
158 and compared them to the whole cell area. Based on the compartment size distribution across  
159 186 cells, for unbiased mRNAs, we expect that 11% of transcripts localize to TGs and 29% of  
160 transcripts localize to the ER (Fig. 1I, 1J).

161 For 3/3 TG+ mRNAs, we observed a significant enrichment of mRNA puncta in TGs, but not on  
162 the ER (Fig. 1G, 1I, 1J, Fig. S2A, S2B, S2H, S2I). For the five ER+ mRNAs tested, the mRNA  
163 puncta of 4/5 mRNAs were significantly enriched on the ER and for all five, we observed a 2-4-  
164 fold higher fraction of mRNA puncta that co-localized with the ER compared to TGs (Fig. 1H-K,  
165 Fig. S2C-I).

166 Cytosolic mRNAs were isolated through digitonin extraction. This means that CY+ mRNAs  
167 localize to the soluble part of the cytoplasm and are not attached to cytoplasmic structures,  
168 including membranes or the cytoskeleton. As steady-state smRNA-FISH can only inform on co-  
169 localization and not attachment, we validated CY+ mRNAs by performing smRNA-FISH before  
170 and after digitonin extraction and calculated the fraction of retained mRNAs. We observed  
171 significantly greater retention of both TG+ and ER+ mRNAs compared to CY+ mRNAs, which  
172 were depleted by about 90% following digitonin treatment (Fig. 1L, 1M, Fig. S3A-C). This  
173 confirms that CY+ mRNAs predominantly localize to the soluble part of the cytoplasm. Taken  
174 together, as we successfully validated 10/11 mRNAs that were designated to be TG+ or ER+ or  
175 CY+ (Fig. 1N), we conclude that about half (52%) of mRNAs encoding non-membrane proteins  
176 are enriched in distinct subcytoplasmic compartments.

177

## 178 **mRNA and protein levels strongly correlate with the location of translation**

179 Next, we characterized the features of compartment-enriched mRNAs and found substantial  
180 differences in their steady-state mRNA and protein levels (Fig. 2A, 2B, Fig. S4A, S4B). We  
181 observed that TG+ mRNAs have the lowest steady-state expression levels and encode proteins  
182 with the lowest expression levels (Fig. 2A, 2B). To examine if the low mRNA levels are caused  
183 by high mRNA degradation rates, we estimated mRNA half-lives by analyzing Precision Run-On  
184 sequencing (Pro-seq) and RNA-seq data (Fig. 2C, 2D, Fig. S4C-E).<sup>27,28</sup> Pro-seq values can be

185 treated as transcription rates and RNA-seq data can be viewed as a measure of RNA  
186 concentration to estimate RNA decay rates required for a steady-state equilibrium.<sup>28</sup> For TG+  
187 mRNAs, we observed that the low steady-state mRNA levels were not primarily caused by a low  
188 mRNA stability. Instead, these mRNAs had the lowest transcription rates, suggesting that these  
189 mRNAs are either produced at a low rate or have high cotranscriptional degradation rates (Fig.  
190 2C, 2D, Fig. S4D, S4E).<sup>29</sup> CY+ mRNAs had the highest degree of mRNA turnover with both  
191 high production and degradation rates (Fig. 2C, 2D). ER+ mRNAs encode proteins with the  
192 highest expression levels, particularly when normalizing to their intermediate steady-state  
193 mRNA levels (Fig. 2A, 2B).

194 In addition, we observed that the compartment-enriched mRNAs differed substantially in their  
195 gene architectures (Fig. 2E-H, Fig. S4F-K). ER+ mRNAs encode the largest proteins with a  
196 median size of 840 amino acids, nearly three-times larger than proteins encoded by CY+  
197 mRNAs (Fig. 2E). The difference in protein size was reflected in the large differences in exon  
198 number and mRNA length between ER+ and CY+ mRNAs (Fig. 2F, Fig. S4J, S4K). The median  
199 length of ER+ mRNAs is 4600 nucleotides (nt), whereas the median length of CY+ mRNAs is  
200 2000 nt. Not surprising, CY+ mRNAs also have the shortest 3'UTRs (Fig. 2G). TG+ mRNAs are  
201 uniquely characterized by large coding sequence (CDS) exons with a median size of 200 nt,  
202 compared to a median exon size of 133 nt for the remaining mRNAs (Fig. 2H). Further analysis  
203 revealed that the majority of TG+ mRNAs have a gene architecture that is similar to the gene  
204 architecture of *ZFP36L1* (encoding TIS11B), which is characterized by a short first exon and a  
205 long last exon that contains ~95% of its coding sequence (Fig. 2I).

206 Moreover, compartment-enriched mRNAs encode substantially different functional gene  
207 classes.<sup>30</sup> Consistent with the low steady-state protein expression levels, TG+ mRNAs were  
208 strongly enriched in proteins containing zinc fingers and in transcription factors, which are  
209 known to have low expression (Fig. 2J).<sup>31</sup> In contrast, ER+ mRNAs encode large and highly  
210 abundant proteins, and they were enriched in helicases, cytoskeleton-binding proteins, and  
211 chromatin regulators (Fig. 2K). CY+ mRNAs often encode smaller proteins involved in the  
212 regulation of translation or splicing (Fig. 2L).

213

## 214 **TGs support active translation**

215 TIS granules may constitute a specialized translation environment for nuclear proteins that  
216 require low expression levels, such as transcription factors (Fig. 2A, 2B, 2J).<sup>31</sup> In order to  
217 provide evidence for active translation in TIS granules, we applied the SunTag system to  
218 simultaneously visualize mRNAs and their nascent proteins in TGs and in the cytosol (Fig. S3D,  
219 S3E).<sup>32</sup> We confirmed that TGs represent a translation environment for mRNAs.<sup>16,19</sup> We  
220 observed that the number of mRNA foci in TGs was five-fold lower compared to the cytosol.  
221 However, the proportion of mRNA translated was similar in TGs and the cytosol (Fig. S3F,  
222 S3G). Taken together, our data show that TGs are sites of active translation and that the low  
223 expression level of TG-translated proteins is predominantly a result of their low nuclear gene  
224 expression (Fig. 2A, 2C).

225

## 226 **Differential 3'UTR binding of several RBPs correlates with compartment enrichment of 227 mRNAs**

228 Our next goal was to identify the RBPs responsible for mRNA enrichment in the three  
229 compartments (Fig. 1D-F). As TIS11B is the scaffold protein of TGs,<sup>16</sup> we performed iCLIP of  
230 TIS11B in HEK293T cells (Fig. S5A, S5B). We confirmed that the top binding motif of TIS11B in  
231 3'UTRs of mRNAs is the canonical AU-rich element (UAUUUA) (Fig. S5C). To perform a

232 comprehensive analysis on localization regulators, we included additional CLIP datasets.<sup>33,34</sup>  
233 Altogether, we analyzed CLIP data from 170 RBPs and found that 24 of them showed an  
234 enrichment of binding sites in 3'UTRs of mRNAs belonging to transcripts that preferentially  
235 localize to one of the three compartments (Table S4). We applied logistic regression and  
236 identified seven RBPs whose binding contributed most significantly to mRNA enrichment in the  
237 three compartments. They include TIS11B, HuR, PUM2, HNRNPC, TIA1/L1, LARP4B and  
238 METAP2 (Fig. 3A). As a previous CLIP analysis showed that peaks for TIA1 and TIAL1 cannot  
239 be distinguished,<sup>35</sup> we used the sum of peaks from TIA1 and TIAL1 to obtain the values for  
240 TIA1/L1. According to this regression analysis, the presence of TIS11B, HuR, PUM2, and  
241 HNRNPC on mRNAs correlates with TG enrichment, the presence of TIA1/L1 correlates with  
242 ER enrichment, and the presence of LARP4B or METAP2 correlates with cytosol enrichment  
243 (Fig. 3A).

244

245 **mRNA architecture features together with RBPs generate a combinatorial code for**  
246 **subcytoplasmic transcript distribution**

247 As our analysis revealed that 2154 mRNAs (30.7%) that encode non-membrane proteins were  
248 not bound by any of the seven RBPs (Fig. S5D), we considered additional regulatory factors for  
249 mRNA localization. Among these mRNAs, we observed that mRNA length correlated strongly  
250 with the ER and CY localization scores, but in opposite directions, suggesting that long mRNAs  
251 are associated with ER localization (Fig. 3B). Similarly, average CDS exon length correlated  
252 strongly and in a positive manner with the TG localization score, but negatively with the CY  
253 localization score (Fig. 3B).

254 When including mRNA and exon length in the logistic regression, we observed that mRNA  
255 architecture features contribute strongly to mRNA enrichment in each of the three  
256 compartments (Fig. 3C, Table S4). Our data indicate that the propensity of an mRNA for  
257 compartment localization depends on both architectural features and the presence of 3'UTR-  
258 bound RBPs. To better understand the rules for mRNA localization to the compartments, we  
259 plotted the propensity for TG enrichment and integrated RBPs that were positively or negatively  
260 associated with TG enrichment together with exon length (Fig. 3D). Regardless of exon length,  
261 binding of LARP4B/METAP2 decreased the TG localization score (Fig. 3D, 3E). For mRNAs  
262 with average exon length, TIS11B binding strongly increased their localization propensity to  
263 TGs. A similar TG localization propensity was observed for mRNAs with long exons that were  
264 not bound by TIS11B. The strongest TG enrichment was found for mRNAs with long exons that  
265 were bound by TIS11B, indicating that TIS11B and exon length have additive effects (Fig. 3D,  
266 3E).

267 The two features that best promote mRNA localization to the ER are mRNA length and 3'UTR-  
268 bound TIA1/L1 (Fig. 3F, 3G). Short mRNAs increase their ER localization propensity by the  
269 presence of TIA1/L1. Long mRNAs that are not bound by TIA1/L1 have a similar propensity for  
270 ER localization, which can be further increased by the presence of TIA1/L1 (Fig. 3F, 3G). In  
271 contrast, shorter mRNAs not bound by any RBP or that are bound by LARP4B/METAP2 have a  
272 high propensity to localize to the cytosolic fraction (Fig. 3G, 3H). Taken together, our data  
273 suggest the existence of a combinatorial code, that integrates mRNA and exon length with the  
274 presence of RBPs, to determine subcytoplasmic mRNA localization (Fig. 3E, 3G).

275

276 **mRNA transcript distribution changes upon TIS11B deletion**

277 Next, we set out to experimentally test the proposed mRNA localization code by investigating  
278 the influence of TIS11B and TIA1/L1 on subcytoplasmic mRNA transcript distribution. We

279 generated HEK293T cells with an inducible knockout (KO) of TIS11B, isolated ER particles and  
280 extracted the cytosol (Fig. S5E, S5F, Table S5). To examine where mRNAs designated as TG+  
281 localize in the absence of TGs, we identified the top 20% of mRNA localization changes to the  
282 ER and the cytosol and intersected them with mRNAs designated as TG+ (Fig. 4A). As only two  
283 compartments were isolated, increased mRNA localization to the ER means decreased  
284 cytosolic localization and vice versa (Fig. 4A).

285 We did not find specific RBPs associated with the localization-changing mRNAs, because TG+  
286 mRNAs are mostly bound by TIS11B and only a small minority of them (13% and 15%) are  
287 LARP4B or TIA1/L1 targets (Table S5). However, the TG+ mRNAs that increased their cytosolic  
288 localization upon TIS11B KO were the shortest, encoded the smallest proteins, and had the  
289 shortest exon length (Fig. 4B-E). In contrast, TG+ mRNAs that increased their ER localization  
290 upon deletion of TIS11B were significantly longer, encoded the largest proteins, and had longer  
291 exons (Fig. 4B-E).

292 These results support a model in which mRNA architecture features set up a ‘default’ steady-  
293 state mRNA transcript distribution pattern in the cytoplasm which can be overcome or reinforced  
294 through the binding of RBPs. Short mRNAs with average exon length localize to TGs when  
295 bound by TIS11B but in the absence of TIS11B they revert to the transcript distribution  
296 established by mRNA architecture and the remaining bound RBPs, in this case the cytosol (Fig.  
297 3E). Similarly, longer TG+ mRNAs that encode the largest proteins localize to the ER upon loss  
298 of TIS11B (Fig. 3G). Currently, the ‘readers’ of the mRNA architecture features are unknown.

299

### 300 **3'UTR-bound TIAL1 promotes localization of non-membrane protein-encoding mRNAs to 301 the ER**

302 We observed that ER+ mRNAs were enriched in 3'UTR-bound TIA1/L1, which had not been  
303 previously reported (Fig. 3A, 3C, 3F). To test the influence of TIA1/L1 on mRNA localization, we  
304 set out to investigate mRNA localization changes to the three compartments in TIA1/L1 double  
305 KO cells.<sup>36</sup> However, as previously reported, these cells showed a high rate of cell death, which  
306 prevented us from obtaining high-quality particles.

307 To validate TIA1/L1-dependent mRNA localization to the ER, we used the MS2 tethering system  
308 to mimic 3'UTR-binding of TIA1/L1 (Fig. 4F). We generated a *GFP-THAP1* reporter mRNA that  
309 contained MS2-binding sites as 3'UTR.<sup>37-39</sup> Coexpression of mCherry-tagged MS2 coat protein  
310 (MCP) fused to TIAL1 tethers TIAL1 to the 3'UTR of the reporter mRNA (Fig. 4F). As a control,  
311 mCherry-tagged MCP was tethered to the *GFP-THAP1* reporter mRNA.

312 Coexpression of the reporter mRNA and MCP resulted in evenly distributed cytosolic expression  
313 of both MCP protein and reporter mRNA (Fig. 4F-H). In contrast, coexpression of the reporter  
314 mRNA and MCP-TIAL1 resulted in perinuclear, reticulated expression of MCP-TIAL1 with the  
315 mRNA reporter predominantly localizing to the rough ER (Fig. 4F-H). Colocalization was  
316 assessed by RNA-FISH of the GFP-tagged reporter mRNA and simultaneous visualization of  
317 the rough ER through fluorescently tagged SEC61B. Using line diagrams of the fluorescence  
318 intensities, we quantified the overlap between the reporter mRNAs and the ER (Fig. 4I). In the  
319 presence of MCP-TIAL1, we observed higher correlation coefficients between the reporter  
320 mRNA and the ER (Fig. 4J). This result indicated that 3'UTR-bound TIAL1 was sufficient to  
321 induce localization of non-membrane protein encoding mRNAs to the rough ER surface.

322

### 323 **3'UTR-bound TIAL1 increases protein expression**

324 For endogenous mRNAs, we observed that ER+ mRNAs encode the highest expressed  
325 proteins (Fig. 2B). Moreover, mRNAs predominantly bound by TIA1/L1 encode proteins with  
326 higher expression levels compared with other mRNAs (Fig. 5A). Using our mRNA reporter (Fig.  
327 4F), we investigated the contribution of TIAL1 to steady-state protein expression. We used  
328 FACS to measure GFP protein expression of the mRNA reporter with or without tethering of  
329 TIAL1 to the 3'UTR (Fig. S6A-C). We observed a 3.5-fold increase in protein expression upon  
330 3'UTR-tethering of TIAL1 compared to tethering of MCP alone (Fig. 5B, 5C). Increased GFP  
331 protein expression was not due to an increase in mRNA abundance (Fig. 5D). We confirmed the  
332 TIA1/L1-dependent increase in protein expression using a second GFP reporter (Fig. S6D-F).  
333 As TIAL1 promotes translation of mRNAs on the ER membrane, it was unclear if increased  
334 protein expression was caused by TIAL1 or by a potentially unique translation environment  
335 provided by the rough ER membrane. For example, it was reported that mRNAs that encode  
336 non-membrane proteins contain 1.4-fold more ribosomes when translated on the ER membrane  
337 than when translated in the cytosol.<sup>40</sup>

338

### 339 **TIAL1 cooperates with the rough ER environment to promote protein expression**

340 To disentangle the effects of TIAL1 and the ER membrane on protein expression, we tethered  
341 the reporter mRNA directly to the ER surface by fusing MCP to SEC61B, a subunit of the  
342 translocon complex in the rough ER (Fig. 5E). MCP-SEC61B perfectly colocalized with the ER  
343 and recruited reporter mRNAs to the ER (Fig. 5F, S6G-I). However, reporter protein expression  
344 only increased by 1.25-fold compared to the tethering of MCP alone and did not increase mRNA  
345 abundance of the reporter (Fig. 5G-I). We used a second ER localization reporter by fusing  
346 MCP to TRAP $\alpha$ , which represents a different subunit of the translocon complex and obtained a  
347 similar result. We observed an increase in protein expression by 1.5-fold when the reporter  
348 mRNA was tethered to TRAP $\alpha$  (Fig. S6J-M). These results suggested that the ER membrane  
349 environment has a significant but small stimulatory effect on translation.

350 Next, we investigated if the TIAL1-dependent increase in protein expression is intrinsic to TIAL1  
351 or if it depends on its localization to the ER membrane. We added a CAAX motif to TIAL1 to  
352 localize the TIAL1-bound mRNA reporter to the plasma membrane instead of the ER membrane  
353 (Fig. 5J). The CAAX signal is a prenylation motif that efficiently localized MCP and MCP-TIAL1  
354 to the plasma membrane (Fig. 5K).<sup>32</sup> Translation of the TIAL1-bound mRNA reporter at the  
355 plasma membrane increased protein expression by 1.8-fold (Fig. 5L, 5M). As translation of the  
356 TIAL1-bound reporter at the ER membrane resulted in two-fold higher protein expression than  
357 its translation at the plasma membrane (Fig. 5M), our result suggested that TIAL1 cooperated  
358 with the environment on the rough ER membrane to promote protein expression.

359 As the RBPs bound to the reporter mRNA were identical in these experiments, our results  
360 demonstrate that the subcytoplasmic location of translation controls steady-state protein  
361 expression levels by two-fold when comparing plasma and ER membranes. This relationship  
362 was also observed for endogenous mRNAs, where TIA/L1 bound mRNAs were associated with  
363 high protein output in every compartment, but with the highest protein yields being observed in  
364 the ER compartment (Fig. 5N).

365

### 366 **The repressive effect of cytosolic TIS11B on protein expression is overcome by its 367 localization to rough ER membrane**

368 Next, we examined if the environment on the rough ER membrane also promotes protein  
369 expression of mRNAs bound by other RBPs, including TIS11B (Fig. 6A, 6B). In cells expressing  
370 mCherry-TIS11B fusion constructs, about 30% form TGs at steady state (Fig. S7A, S7B).<sup>16</sup>

371 However, we noticed that addition of MCP to TIS11B fusion constructs resulted in limited TG  
372 formation and predominant expression of TIS11B in the cytosol (Fig. S7A, S7B). In the cytosolic  
373 state, binding of MCP-TIS11B to the reporter mRNA repressed reporter protein expression by  
374 two-fold, compared to tethering of MCP alone (Fig. 6C, 6D). This decrease in protein expression  
375 was partially caused by a TIS11B-dependent decrease in mRNA level (Fig. 6E), consistent with  
376 previous reports that suggested that cytosolic TIS11B represses the expression of certain  
377 cytokine and cell cycle mRNAs.<sup>41-43</sup> In contrast, fusing TIS11B to MCP-SEC61B localizes  
378 TIS11B and the bound reporter mRNA to the rough ER (Fig. 6A, 6B), which overcomes the  
379 repressive effect of cytosolic TIS11B and increased protein expression two-fold (Fig. 6A-E). The  
380 two-fold increase in protein expression was recapitulated with a second reporter and indicates  
381 that the repressive effect on protein expression mediated by cytosolic TIS11B is overcome by  
382 translation of the TIS11B-bound mRNA on the ER (Fig. 6D, Fig. S7C-E).

383

#### 384 **Model**

385 Taken together, we observed that mRNAs that are uniquely enriched in one of three  
386 cytoplasmic compartments differ substantially in their architectural features, in the RBPs bound  
387 to them, and in the expression levels and functional classes of their encoded proteins (Fig. 7).  
388 TG+ mRNAs are characterized by the longest CDS exons and TIS11B binding to the 3'UTR.  
389 These mRNAs encode the lowest abundance proteins with a strong enrichment of transcription  
390 factors. In contrast, although TGs are intertwined with the rough ER, ER+ mRNAs are the  
391 longest, are predominantly bound by TIA1/L1, and encode highly abundant large proteins. CY+  
392 mRNAs are the shortest and encode small and highly abundant proteins. They are bound by  
393 LARP4B/METAP2 and have high production and degradation rates (Fig. 7). Moreover, by using  
394 mRNA reporters, we showed that relocation of protein synthesis from the cytosol to the ER  
395 increases protein expression, indicating that the location of translation influences protein output  
396 (Fig. 7).

397

398

#### 399 **Discussion**

400 We determined the distribution of endogenous mRNA transcripts across three cytoplasmic  
401 compartments, including TGs, the rough ER, and the cytosol under steady-state conditions. Our  
402 RNA-seq results, which were validated by smRNA-FISH, suggest that approximately half of all  
403 mRNAs are uniquely enriched in one of these three cytoplasmic compartments.

404

#### 405 **Functionally related genes are translated in unique compartments**

406 One of our most striking findings was that within each investigated compartment a different  
407 group of functionally related mRNAs is translated (Fig. 2). Moreover, the compartment-enriched  
408 mRNAs have vastly different gene architectures and are characterized by substantially different  
409 production and degradation rates as well as the expression levels of their encoded proteins (Fig.  
410 2). These features are consistent with the compartment-enriched gene groups, indicating that  
411 the cytoplasm is strongly partitioned into different functional and regulatory compartments that  
412 are not enclosed by membranes.

413 Surprisingly, we observed that transcription factors are substantially enriched among TG+  
414 mRNAs (Fig. 2J). This unexpected result can be explained by the previous observation that  
415 transcription factors are often present in low abundance<sup>31</sup> and we found that TG+ mRNAs  
416 encode the proteins with the lowest expression levels (Fig. 2B). Moreover, many transcription

417 factors have an unusual gene architecture with longer than average coding exons. Together  
418 with TIS11B binding, this was the strongest feature for mRNA enrichment in TGs (Fig. 3C-E).  
419 Interestingly, both characteristics correlate with features associated with low mRNA abundance  
420 levels, but whereas TIS11B-binding correlates negatively with pre-mRNA production rates  
421 (Spearman's correlation coefficient  $R = -0.26$ ), exon length negatively correlates with mRNA  
422 half-life (Spearman's correlation coefficient  $R = -0.34$ ).<sup>44</sup> The unique gene architecture together  
423 with predominant binding of TIS11B provides an explanation for why TGs enrich for low-  
424 abundance mRNAs.

425 In contrast, ER+ mRNAs encode the largest proteins with the highest expression levels. These  
426 include helicases, cytoskeleton-bound proteins, and chromatin regulators (Fig. 2). It is possible  
427 that anchoring of ribosomes on the ER membrane may facilitate the protein synthesis of very  
428 large proteins. Moreover, it is notable that despite the intertwinement of TGs and the rough ER,  
429 the compartment-enriched mRNAs encode proteins that differ substantially in their expression  
430 levels, which are the lowest for TG+ mRNAs and the highest for ER+ mRNAs.

431 It was previously shown that localization to the ER membrane of certain non-membrane protein  
432 encoding mRNAs increases their translation,<sup>9,40</sup> and we confirmed this result. In addition, we  
433 describe a new role for TIAL1 in the regulation of translation, as TIAL1 binding substantially  
434 increased mRNA translation (Fig. 5C). So far, TIA1 and TIAL1 have mostly been described as  
435 regulators of pre-mRNA splicing and as translational repressors in the context of cellular stress,  
436 where they assemble into stress granules.<sup>45,46</sup> However, in the absence of stress, TIA1/L1 has  
437 been reported to promote polysome association which supports our findings.<sup>36,47</sup> For both  
438 reporter mRNAs and endogenous mRNAs, we observed that the presence of TIAL1 increased  
439 protein expression in all compartments, but only in the context of the ER did we observe a  
440 cooperative effect on translation (Fig. 5M, 5N). The factor that cooperates with TIAL1 on the ER  
441 to upregulate translation is currently unknown. Importantly, our reporter results demonstrate that  
442 a change in the location of protein synthesis within the cytoplasm strongly influences protein  
443 output, indicating that a change in mRNA localization can alter protein abundance.

444

#### 445 **A combinatorial code of mRNA architecture features and 3'UTR-bound RBPs controls** 446 **subcytoplasmic mRNA transcript distribution**

447 RBPs play an established role in mRNA localization.<sup>1,7</sup> Additionally, we observed a strong  
448 association of mRNA architecture features with mRNA transcript localization to the three  
449 cytoplasmic compartments (Fig. 3C). It is most likely that mRNA length, CDS length, and CDS  
450 exon length are not direct regulators of mRNA localization but that specific factors, including  
451 currently unknown RBPs, read-out this information. In addition, we speculate that mRNA  
452 architecture influences mRNP size, conformation, and packaging<sup>48,49</sup> and that these biophysical  
453 features may act as additional determinants of subcytoplasmic mRNA localization. This idea is  
454 supported by previous insights into *oskar* mRNA localization, where the deposition of the exon  
455 junction complex, which is involved in mRNP packaging,<sup>48,49</sup> was found to be required for  
456 proper mRNA localization in the cytoplasm.<sup>50</sup>

457 We present a model for the regulation of subcytoplasmic transcript distribution that is based on  
458 a combinatorial code generated by mRNA architecture features together with the bound RBPs,  
459 where individual components act in an additive manner (Fig. 3E, 3G). This model was tested  
460 experimentally by analyzing the localization propensity of TG+ mRNAs upon deletion of TIS11B.  
461 The obtained results confirmed the contribution of mRNA architectural features to mRNA  
462 localization and suggest that the binding of RBPs can overcome the default localization pattern  
463 established by the mRNA architecture features (Fig. 4A-E).

464

465 **Is it biologically relevant if only 20% of transcripts localize to TGs?**

466 Based on the estimated size of TGs (Fig. 1I), we expect that 11% of mRNA transcripts localize  
467 to TGs by chance. Using smRNA-FISH on three individual TG+ mRNAs we observed a two-fold  
468 enrichment in TGs, meaning that on average 22% of these transcripts localize to TGs. This  
469 raises the important question: whether it matters biologically that a minority population of  
470 transcripts for a given mRNA localizes to a certain compartment.

471 This question was addressed in a follow-up project, where we investigated the biological  
472 consequences of *MYC* mRNA, which is a TG+ mRNA, when it was translated in TGs or the  
473 cytosol.<sup>19</sup> We observed that several *MYC* protein complexes were only formed when *MYC*  
474 mRNA was translated in TGs and not when it was translated in the cytosol. The TG-dependent  
475 protein complexes formed co-translationally and had functional consequences for *MYC* target  
476 gene expression in the nucleus. TG-translated *MYC* induced different target genes than cytosol-  
477 translated *MYC*.<sup>19</sup> Our results indicate biological relevance, even when only a fraction of  
478 transcripts are translated in TGs.

479 In summary, our study revealed a surprisingly high degree of cytoplasmic compartmentalization.  
480 This is the basis for the translation of functionally related proteins in defined environments that  
481 strongly affect mRNA and protein expression. Our results highlight the contribution of spatial  
482 regulation whose consequences go beyond the effects mediated by the mRNA-bound proteins.  
483 In the future, our findings may provide the basis for biotechnology applications that make use of  
484 engineered 3'UTR sequences to boost protein expression in experimental settings or to  
485 increase protein production of mRNA vaccines.

486

487 **Limitations of our study**

488 The exact compartment sizes of TGs, the rough ER, and the cytosol are currently unknown and  
489 can only be estimated. However, using two different methods for the identification of  
490 compartment-enriched mRNAs yielded highly similar enrichment values.

491 To obtain sufficient material for TG and ER particle sorting, we used transfected, fluorescently  
492 labeled proteins instead of endogenous proteins. In cells that highly express TIS11B, in the  
493 future, TG particle sorting may be possible using endogenous, fluorescently tagged TIS11B.

494 The use of spike-ins to isolated compartments obtained from defined cell numbers may have  
495 enabled us to perform absolute enrichments versus the relative enrichment analyses that we  
496 report here. Moreover, all analyses were performed at the gene level. Alternative 3'UTR  
497 isoforms are known to differentially localize and therefore, we would expect to obtain a higher  
498 resolution for compartment enrichment of transcripts if instead of genes alternative 3'UTR  
499 isoforms are analyzed.<sup>38,51</sup> However, with our purification strategy we did not obtain sufficient  
500 mRNA quantities to perform the analysis at the level of alternative 3'UTR isoforms.

501

502

503 **Acknowledgements**

504 This work was funded by the NIH Director's Pioneer Award (DP1-GM123454), the  
505 R35GM144046 NIH grant, a grant from the Pershing Square Sohn Cancer Research Alliance, a  
506 grant from the G. Harold and Leila Y. Mathers Foundation, and the MSK Core Grant (P30  
507 CA008748) to CM. J.U. received funding from the ERC under the European Union Horizon  
508 2020 Research and Innovation Program (835300-RNPdynamics) and The Francis Crick Institute

509 receives its core funding from Cancer Research UK (CC0102), the UK Medical Research  
510 Council (CC0102), and the Wellcome Trust (CC0102). An NIH F31 (CA254335-01) fellowship  
511 was awarded to E.L.H.

512 We thank Yevgeniy Romin and Eric Chan from the Molecular Cytology Core Facility for help  
513 with microscopy and image analysis. We thank Kathleen Daniels from the Flow Cytometry Core  
514 Facility (now Sana Biotechnologies) for help with particle sorting and Liana Boraas at Yale  
515 University School of Medicine for help with endogenous RNA-FISH. We thank Weirui Ma  
516 (Zhejiang University) for experimental guidance and mentorship of E.L.M. and Alban Ordureau  
517 for analysis of the TMT mass spectrometry data. We thank Yang Luo (MSKCC) and Ben  
518 Kleaveland (WCMC) for helpful discussions and critical reading of the manuscript.

519

## 520 **Author contributions**

521 E.L.H. performed all experiments, except the mass spectrometry analysis whose samples were  
522 prepared by X.C. and the TIS11B KO cells were generated by S.M. F.C.Y.L. and J.U. performed  
523 and analyzed the TIS11B iCLIP experiment. M.M.F performed the logistic regression and  
524 provided the gene architecture features. T.C. analyzed the RNA-seq data. G.Z. analyzed the  
525 CLIP data with input from C.M. E.L.H. and C.M. conceived the project, designed the  
526 experiments, and wrote the manuscript with input from all authors.

527

## 528 **Declaration of Interests**

529 The authors declare no competing interests.

530

531

532

533

534

535 **Methods**

536 **STAR methods table**

537 **Cell lines**

538 **Generation of a doxycycline inducible *TIS11B* knockout cell line (*TIS11B* KO)**

539 Doxycycline inducible Cas9 (iCas9) HEK293T cells were generated by infecting cells with  
540 lentivirus containing a Cas9-P2A-GFP expression cassette under a doxycycline inducible  
541 promoter as described previously.<sup>52</sup> During consecutive rounds of fluorescence-activated cell  
542 sorting, we selected a cell pool exhibiting robust induction of Cas9/GFP expression after  
543 doxycycline treatment (100 ng/ml for 24 hours), and low levels of leaky transgene expression in  
544 the absence of the drug.

545 Next, we transduced iCas9 cell lines with a lentiviral construct harboring a pair of guide RNAs  
546 either targeting *TIS11B* or gRNAs that target an intergenic region. To generate these constructs,  
547 we adapted the plentiGuide-puro vector.<sup>53</sup> to incorporate a second guide RNA expression  
548 cassette as described previously.<sup>54</sup> For this purpose, the plasmid was digested with BsmBI  
549 (FastDigest Esp3I, Thermo Fisher Scientific) and a synthetic 391 bp double-stranded DNA  
550 fragment encoding 5'-(1st gRNA/scaffold/H1 promoter/2nd gRNA)-3' was inserted using the  
551 NEBuilder HiFi assembly system (NEB). Synthetic DNA fragments were ordered from Genewiz  
552 and sequences are listed in Table S6. The assembled vector DNA was used to transform  
553 chemically competent Stbl3 bacteria cells (Invitrogen), and correct vector clones were identified  
554 by Sanger sequencing.

555 Lentivirus was generated in HEK293T cells using standard methods and 200 µl of viral  
556 supernatant was used to transduce iCas9 cells in a 6-well dish together with 8 µg/ml polybrene.  
557 Transduced cells were subjected to puromycin selection (1 µg/ml) for five days and resistant  
558 cells were aliquoted and frozen for all further experiments. Finally, for induction of gene  
559 knockouts, *TIS11B* KO and corresponding control cells (with gRNAs targeting an intergenic  
560 region) were treated with doxycycline (100 ng/ml) for five days, after which TIS11B protein  
561 expression was evaluated by western blotting, ER particle sorting and digitonin extraction was  
562 performed.

563

564 **Detailed methods**

565 **Constructs**

566 Fluorescently-tagged TIS11B and SEC61B constructs. The eGFP/mCherry/BFP fusion  
567 constructs for TIS11B and SEC61B expression were described previously.<sup>16</sup> They were  
568 generated in the pcDNA3.1-puro expression vector. The TIS11B and SEC61B coding regions  
569 were PCR amplified from HeLa cDNA and inserted downstream of eGFP/mCherry/BFP using  
570 BsrGI/EcoRI or BsrGI/HindIII restriction sites, respectively.

571 Constructs to generate the mRNA localization reporter. To investigate the influence of RBPs on  
572 mRNA localization of a GFP mRNA reporter, RBPs were fused to MCP and tethered to a GFP  
573 mRNA reporter containing MS2 binding sites as 3'UTR.<sup>37,38</sup> To investigate mRNA localization-  
574 dependent protein expression of the GFP mRNA reporter, a CAAX sequence was fused to MCP  
575 or to MCP-RBP fusions.

576 GFP mRNA reporter. To generate the GFP mRNA reporter, the GFP-BIRC3-MS2-SU<sup>39</sup> vector  
577 was used the BIRC3 coding region was replaced with the THAP1 coding region. It was PCR  
578 amplified from the GFP-THAP1 vector using THAP1-MS2 F and THAP1-MS2 R primers and

579 inserted between the BsrGI and AgeI sites. The SU fragment was removed with HindIII and  
580 Xhol and blunt end ligated, resulting in GFP-THAP1-MS2.

581 MCP-mCherry RBP fusion constructs. To generate MCP-mCherry, the MCP coding sequence  
582 was PCR amplified from UBC NLS-HA-2XMCP-tagRFPt vector (Addgene 64541) using MCP F  
583 and MCP R primers and inserted in-frame, upstream of mCherry (mCherry lacking a start  
584 codon) between Bmtl and BamHI sites in pcDNA3.1-puro-mCherry vector.<sup>16</sup> To generate MCP-  
585 mCherry-TIS11B and MCP-mCherry-TIAL1, their coding sequences were inserted in-frame,  
586 downstream of mCherry between the BsrGI and XbaI sites. The TIS11B coding sequence was  
587 amplified from pcDNA3.1-puro-GFP-TIS11B using TIS11B MCP F and TIS11B MCP R primers  
588 and the TIAL1 coding sequence was PCR amplified from pFRT\_TO\_FlagHA\_TIAL1 (Addgene  
589 106090) using TIAL1 MCP F and TIAL1 MCP R primers.

590 MCP-mCherry fusion constructs with subcellular localization signals. To generate pcDNA3.1-  
591 puro-MCP-mCherry-SEC61B, the MCP-mCherry coding sequence was cut from MCP-mCherry  
592 vector using Bmtl and BsrGI and pasted in-frame, upstream of SEC61B in pcDNA3.1-mCherry-  
593 SEC61B (replacing mCherry). To generate the TIS11B-MCP-mCherry-SEC61B vector, TIS11B  
594 coding sequence was PCR amplified from pcDNA3.1-puro-GFP-TIS11B using TIS-SEC F and  
595 TIS-SEC R primers and pasted in-frame, upstream of MCP into the Bmtl site in the MCP-  
596 mCherry-SEC61B vector. To generate TRAP $\alpha$ -MCP-mCherry, the TRAP $\alpha$  coding sequence  
597 (encoded by the SSR1 gene) was PCR amplified from HeLa cDNA using TRAP $\alpha$  MCP F and  
598 TRAP $\alpha$  MCP R and inserted in-frame, upstream of MCP in the pcDNA3.1-puro-MCP-mCherry  
599 vector.

600 For plasma membrane localization, the CAAX prenylation signal was added to the C-terminus of  
601 MCP-mCherry or MCP-mCherry-TIAL1. The CAAX coding sequence was purchased as a gene  
602 fragment from Azenta as described<sup>32</sup> and PCR amplified using TIAL1 CAAX F and CAAX R  
603 primers. It was inserted in-frame using the BsrGI and Apal sites, located downstream of  
604 mCherry to generate pcDNA3.1-puro-MCP-mCherry-CAAX. It was inserted in-frame using  
605 EcoNI and Apal sites to generate MCP-mCherry-TIAL1-CAAX.

606 SunTag constructs were described previously.<sup>32</sup>

### 607 Isolation of subcytoplasmic compartments

608 Transfection. HEK293T cells were seeded in six 10 cm dishes (particle sorting) or one well from  
609 a 6-well plate (cytosol extraction) at 80% confluence in antibiotic free media. After 24 hours,  
610 cells were transfected by calcium phosphate with either 3  $\mu$ g mCherry-TIS11B or 1  $\mu$ g GFP-  
611 SEC61B per dish (particle sorting), or 500ng mCherry-TIS11B (cytosol extraction).

612 Particle purification. 20 hours after transfection, cells were rinsed once with ice-cold PBS,  
613 scraped in 10 ml ice-cold PBS, and pelleted at 300 x g. Pellets from two plates were  
614 resuspended in 1 ml ice-cold hypotonic isolation buffer (225 mM mannitol, 75 mM sucrose, 20  
615 mM Tris-HCl pH 7.4, 0.1 mM EDTA). Cells were lysed with 50 strokes in a 1 ml dounce-  
616 homogenizer with pestle on ice in order to shear the nuclei from the ER. Nuclei were pelleted  
617 with a two-minute spin at 600 x g. The supernatant contains the cytoplasmic membrane fraction,  
618 which was pelleted with a 15-minute spin at 7000 x g and resuspended in ice-cold PBS for  
619 fluorescent particle sorting.

620 Fluorescent particle sorting. Particles were sorted on a BD FACSAria III cell sorter equipped  
621 with a 70  $\mu$ m nozzle. The forward-scatter threshold was decreased from 5,000 to 800 in order to  
622 visualize subcellular particles. Particles were first detected by fluorescence using the 594 nm  
623 and 488 nm excitation lasers, for mCherry-TIS11B and GFP-SEC61B respectively, and 405 nm  
624 excitation laser for DAPI. A sorting gate was drawn on particles that were either mCherry-  
625 positive or GFP-positive, but DAPI-negative, to exclude any remaining nuclei. Sorting was

626 performed in purity mode with an average speed of 150 particles/second. Particles were sorted  
627 directly into 1 ml of TRIzol solution in Eppendorf tubes, holding 180,000 particles per tube. RNA  
628 extraction was performed for each tube separately and total RNA for each sample was  
629 combined for library preparation. Two biological replicates for each particle prep were  
630 sequenced. For each replicate, about 1.5 million TIS11B granule particles and 2.0 million ER  
631 particles were collected.

632 Cytosol extraction. The cytosol was extracted as previously described.<sup>24</sup> HEK293T cells  
633 transfected were plated in a six-well plate at 80% confluence. After 24 hours, cells were rinsed  
634 once in the dish with ice-cold PBS. After aspirating PBS, 300 µl ice-cold digitonin solution (40  
635 µg/ml digitonin, 150 mM NaCl, 20 mM HEPES pH 7.4, 0.2 mM EDTA, 2 mM DTT, 2 mM MgCl<sub>2</sub>)  
636 was added and incubated on a shaker at 4°C for ten minutes. After incubation, the digitonin-  
637 derived cytosolic extract was pipetted from the plate and spun at 20,000 x g for one minute to  
638 pellet any floating cells. 200 µl of cytosolic extract was added to 1 ml TRIzol solution for RNA  
639 extraction.

#### 640 **RNA-seq library preparation**

641 RiboGreen RNA Reagent (ThermoFisher) was used for RNA quantification and quality control  
642 was performed by Agilent BioAnalyzer. 50-500 ng of total RNA underwent polyA selection and  
643 TruSeq library preparation according to instructions provided by Illumina (TruSeq Stranded  
644 mRNA LT Kit, catalog # RS-122-2102), with eight cycles of PCR. Samples were barcoded and  
645 run on a HiSeq 4000 in a PE50 run, using the HiSeq 3000/4000 SBS Kit (Illumina). An average  
646 of 27 million paired reads was generated per sample.

#### 647 **Western Blotting**

648 For whole cell lysate preparation, cells were trypsinized and washed twice with PBS and lysed  
649 in 2x Laemmli Sample buffer (Alfa Aesar, J61337). For cytosolic lysate, cytosol was extracted  
650 with digitonin as described above and one volume of 2x Laemmli Sample buffer was added.  
651 Laemmli lysates were boiled for 10 min at 95°C. Samples were subjected to SDS-PAGE on  
652 NuPAGE 4%-12% Bis-Tris gradient protein gel (Invitrogen). Imaging was captured on the  
653 Odyssey DLx imaging system (Li-Cor). Quantification was performed using ImageJ. The  
654 antibodies used are listed in the Key Resources Table.

#### 655 **TIS11B iCLIP**

656 Transfection. HEK293T cells were seeded in 10 cm dishes at 80% confluence in antibiotic free  
657 media. After 24 hours, cells were transfected by calcium phosphate with either 3 µg GFP-  
658 TIS11B or 1.5 µg GFP-only per dish.

659 Sample preparation. 20 hours after transfection, cells were rinsed once with ice-cold PBS and 6  
660 ml of fresh PBS was added to each plate before crosslinking. Cells were irradiated once with  
661 150 mJ/cm<sup>2</sup> in a Spectroline UV Crosslinker at 254 nm. Irradiated cells were scraped into  
662 Eppendorf tubes, spun at 500 x g for one minute, and snap-frozen. Crosslinked cell pellets were  
663 lysed in iCLIP lysis buffer (50 mM Tris-HCl pH 7.4, 100 mM NaCl, 1% Igepal CA-630 (Sigma  
664 I8896), 0.1% SDS, 0.5% sodium deoxycholate), sonicated with the Bioruptor Pico for 10 cycles  
665 30 seconds ON/30 seconds OFF, and supplemented with 0.5 U of RNase I per 1 mg/ml lysate  
666 for RNA fragmentation. Lysates were pre-cleared by centrifugation at 20,000 x g at 4°C. A mix  
667 of Protein A/G Dynabeads (50 µl of each per sample, Life Technologies) were coupled to 10 µg  
668 of rabbit anti-GFP antibody (Abcam ab290). TIS11B protein-RNA complexes were  
669 immunoprecipitated from 1 ml of crosslinked lysate and washed with high salt and PNK buffer  
670 (NEB). RNA was repaired by 3' dephosphorylation and ligated to L3-IR adaptor on beads.<sup>55</sup>  
671 Excess adaptor was removed by incubation with 5' deadenylase and the exonuclease RecJf  
672 (NEB). TIS11B protein-RNA complexes were eluted from the beads by heating at 70°C for one

673 minute. The complexes were then visualized via the infrared-labeled adaptor, purified with SDS-  
674 PAGE, and transferred to nitrocellulose membrane. cDNA was synthesized with Superscript IV  
675 Reverse Transcriptase (Life Technologies) and circularized by CircLigase II. Circularized cDNA  
676 was purified with AmPURE bead-based purification (A63880, Beckman Coulter), amplified by  
677 PCR and sequenced by Novaseq.

678 **RNA-FISH**

679 Single molecule RNA-FISH for endogenous mRNAs. Probe design. Primary probes were  
680 designed using the ProbeDealer package in MATLAB.<sup>56</sup> Each primary probe contains 30  
681 transcript-targeting nucleotides preceded by 20 common nucleotides that are complementary to  
682 the secondary probe. At least 30 probes were designed for each transcript, purchased in a pool  
683 from IDT. The secondary probes are 5' conjugated to AlexaFluor 633 and were purchased from  
684 IDT.

685 Transfection. Prior to cell seeding, 35 mm glass cover slips were sterilized with ethanol then  
686 incubated in 1 µg/ml fibronectin in PBS at room temperature for one hour. Cover slips were  
687 rinsed in PBS and HeLa cells were seeded at 100,000 per coverslip. 24 hours after seeding,  
688 cells were co-transfected with 250 ng BFP-TIS11B and 100ng of GFP-SEC61B using  
689 Lipofectamine 3000 (Invitrogen).

690 Sample preparation. 20 hours after transfection, cells were rinsed once with PBS then fixed in  
691 4% paraformaldehyde for 10 minutes at room temperature. All steps were performed at room  
692 temperature if not otherwise noted. Cells were rinsed twice with PBS and permeabilized with  
693 0.5% Triton-X solution for 10 minutes. Cells were rinsed twice with PBS and incubated for five  
694 minutes in pre-hybridization buffer (2xSSC, 50% formamide). Cells were incubated in primary  
695 probe hybridization solution (40 µM primary probe, 2xSSC, 50% formamide, 10% dextran  
696 sulfate (Sigma), 200 µg/ml yeast tRNA (Sigma), 1:100 Murine RNase Inhibitor (NEB)), for at  
697 least 15 hours at 37°C. To remove excess or unbound primary probes, cells were then rinsed  
698 twice in 2xSSC + 0.1% Tween for 15 minutes at 60°C then once more for 15 minutes at room  
699 temperature. Cells were incubated in secondary probe solution (4 nM secondary probe, 2xSSC,  
700 50% ethylene carbonate, 1:100 Murine RNase Inhibitor) for 30 minutes in the dark. Secondary  
701 probes were rinsed twice in 50% ethylene carbonate, 2xSSC solution for five minutes then  
702 mounted with Prolong Diamond mounting solution (Invitrogen).

703 Cytosol extraction. To visualize and validate CY+ versus TG+ or ER+ endogenous mRNAs,  
704 HeLa cells were seeded as described above, then incubated in 2 ml digitonin solution described  
705 above (40 µg/ml digitonin, 150 mM NaCl, 20 mM HEPES pH 7.4, 0.2 mM EDTA, 2 mM DTT, 2  
706 mM MgCl<sub>2</sub>) for 10 min at 4°C. Digitonin solution was removed, coverslips were rinsed with 2 ml  
707 PBS, and RNA-FISH was performed as described above. Mounting media with DAPI was used  
708 to visualize nuclei (Invitrogen P36931).

709 Validation of TG+ and ER+ mRNAs using smRNA-FISH. We performed smRNA-FISH on  
710 endogenous mRNAs (Table S2) while simultaneously visualizing TGs and the ER. We  
711 considered an mRNA to have an unbiased localization pattern if its transcript distribution  
712 correlated with the cytoplasmic compartment sizes. As a proxy for the relative compartment  
713 sizes, we used the area occupied by TGs or the ER compared to the whole cell area, obtained  
714 from the maximum projection of the fluorescent signals in 186 cells. We used FIJI to delineate  
715 the whole cell border with the fluorescent signal from RNA-FISH. For TGs, the fluorescent signal  
716 from BFP-TIS11B and for the ER the fluorescent signal from GFP-SEC61B both obtained from  
717 the maximum intensity Z-projections was used to delineate each compartment. Where there  
718 was overlap between the TG mask and the ER mask, the ER was subtracted, and the region  
719 was defined as TG. In this way the compartments are mutually exclusive. The mask area of  
720 each compartment was quantified and read out as a proportion of the total cell area. Across all

721 cells, the median size of TGs was estimated to be 11% of the cell size, whereas the median ER  
722 size was estimated to be 29% of the cell size (Fig 1I, 1J). Therefore, for mRNAs with an  
723 unbiased transcript distribution, we expect that typically 11% of transcripts colocalize with TGs  
724 and 29% colocalize with the ER.

725 To determine mRNA transcripts enriched in TG or ER, smRNA-FISH foci were counted using  
726 the maxima function and the total number of foci per cell are quantified. Next, all foci are  
727 overlaid with the TG mask and the ER mask to identify mRNAs that colocalize with each  
728 compartment. To determine if an mRNA is compartment enriched, we tested if its observed  
729 compartment distribution differs from the expected distribution based on compartment size  
730 using a Mann Whitney test. The code for the image analysis is available (see below).

731 Of note, this analysis does not distinguish between nuclear and cytoplasmic mRNA localization.  
732 For 7/8 mRNAs this does not influence the outcome because the mRNA signal in the nucleus is  
733 negligible or non-existent. However, smRNA-FISH probes for endogenous *TES* produce high  
734 nuclear background signal. In this case, the prominence value, used to define local maxima to  
735 call foci, is increased such that nuclear noise does not substantially influence foci quantification  
736 (Fig. S2G).

737 Validation of CY+ mRNAs by smRNA-FISH after digitonin extraction. To distinguish CY+  
738 mRNAs from TG+ or ER+ mRNAs, we performed smRNA-FISH on endogenous mRNAs in  
739 untreated and digitonin treated cells, as previously reported.<sup>57</sup> The total number of mRNA foci  
740 per cell is calculated using the maxima function in FIJI. Next, thresholding is applied to DAPI  
741 fluorescence to generate a nuclear mask. Total mRNA foci are overlaid with the DAPI mask and  
742 nuclear foci are subtracted from the total, yielding cytoplasmic foci. Cytoplasmic foci are  
743 quantified for at least 10 cells per condition per experiment. For each experiment, the mean  
744 fraction of transcripts retained is calculated as the average cytoplasmic foci per digitonin-treated  
745 cell divided by the average cytoplasmic foci per untreated cell. At least three separate  
746 experiments per mRNA were performed.

747 RNA-FISH after transfection of constructs. RNA-FISH experiments probing for GFP-fusion  
748 constructs were performed as described previously.<sup>16</sup> Stellaris FISH probes for eGFP with  
749 Quasar 670 Dye were used.

750 Line profile analysis. To quantify colocalization of ER (GFP-SEC61B) and mRNA (AF633)  
751 fluorescence signals, line profiles were generated with FIJI (ImageJ). For each cell, 2-4 straight  
752 lines were drawn to cross the ER in different directions, indicated by the white arrows shown in  
753 the figures. Fluorescence signal along the straight line of the ER and the mRNA reporter was  
754 calculated for each channel using the plot profile tool in FIJI. The values of the Pearson's  
755 correlation coefficient r were calculated using Excel. Perfect correlation of protein-mRNA is  
756 indicated by r = 1, perfect exclusion is indicated by r = -1, and random distribution is indicated  
757 by r = 0.

758

## 759 **Confocal microscopy**

760 Confocal imaging was performed using ZEISS LSM 880 with Airyscan super-resolution mode or  
761 Nikon CSU-W1 with SoRa super-resolution mode. A Plan-Apochromat 63x/1.4 (Zeiss) or  
762 60x/1.49 (Nikon) Oil objective was used. For live cell imaging, cells were incubated with a  
763 LiveCell imaging chamber (Zeiss, Nikon) at 37°C and 5% CO<sub>2</sub> and imaged in cell culture media.  
764 Excitations were performed sequentially using 405, 488, 594 or 633 nm laser wavelength and  
765 imaging conditions were experimentally optimized to minimize bleed-through. Z-stack images  
766 were captured with the interval size of 0.2 μm. Images were prepared with FIJI (ImageJ)  
767 software.

768

769 **TMT mass spectrometry**

770 To obtain protein expression levels, TMT mass spectrometry analysis was performed on  
771 HEK293T cells cultivated in steady-state conditions. Cells were trypsinized and washed three  
772 times with ice-cold PBS. Pelleted cells were snap-frozen in liquid nitrogen. Cell pellets were  
773 lysed with 200 µl buffer containing 8 M urea and 200 mM EPPS (pH at 8.5) with protease  
774 inhibitor (Roche) and phosphatase inhibitor cocktails 2 and 3 (Sigma). Benzonase (Millipore)  
775 was added to a concentration of 50 µg/ml and incubated at room temperature for 15 min  
776 followed by water bath sonication. Samples were centrifuged at 14,000 g at 4°C for 10 min, and  
777 supernatant extracted. The Pierce bicinchoninic acid (BCA) protein concentration assay was  
778 used to determine protein concentration. Protein disulfide bonds were reduced with 5 mM tris  
779 (2-carboxyethyl) phosphine at room temperature for 15 min, and alkylated with 10 mM  
780 iodoacetamide at room temperature for 30 min in the dark. The reaction was quenched with 10  
781 mM dithiothreitol at room temperature for 15 min. Aliquots of 100 µg were taken for each sample  
782 and diluted to 100 µl with lysis buffer. Samples were subject to chloroform/methanol  
783 precipitation as previously described.<sup>58</sup> Pellets were reconstituted in 200 mM EPPS buffer and  
784 digested with Lys-C (1:50 enzyme-to-protein ratio) and trypsin (1:50 enzyme-to-protein ratio),  
785 and digested at 37°C overnight.

786 Peptides were TMT-labeled as described.<sup>58</sup> Briefly, peptides were TMT-tagged by the addition  
787 of anhydrous ACN and TMTPro reagents (16plex) for each respective sample and incubated for  
788 1 hour at room temperature. A ratio check was performed by taking a 1 µl aliquot from each  
789 sample and desalted by StageTip method<sup>59</sup>. TMT tags were then quenched with hydroxylamine  
790 to a final concentration of 0.3% for 15 min at room temperature. Samples were pooled 1:1  
791 based on the ratio check and vacuum-centrifuged to dryness. Dried peptides were reconstituted  
792 in 1 ml of 3% ACN/1% TFA, desalted using a 100 mg tC18 SepPak (Waters), and vacuum-  
793 centrifuged overnight.

794 Peptides were centrifuged to dryness and reconstituted in 1 ml of 1% ACN/25mM ABC.  
795 Peptides were fractionated into 48 fractions. Briefly, an Ultimate 3000 HPLC (Dionex) coupled to  
796 an Ultimate 3000 Fraction Collector using a Waters XBridge BEH130 C18 column (3.5 um 4.6 x  
797 250 mm) was operated at 1 ml/min. Buffer A, B, and C consisted of 100% water, 100% ACN,  
798 and 25mM ABC, respectively. The fractionation gradient operated as follows: 1% B to 5% B in  
799 1 min, 5% B to 35% B in 61 min, 35% B to 60% B in 5 min, 60% B to 70% B in 3 min, 70% B to  
800 1% B in 10 min, with 10% C the entire gradient to maintain pH. The 48 fractions were then  
801 concatenated to 12 fractions, (i.e. fractions 1, 13, 25, 37 were pooled, followed by fractions 2,  
802 14, 26, 38, etc.) so that every 12<sup>th</sup> fraction was used to pool. Pooled fractions were vacuum-  
803 centrifuged and then reconstituted in 1% ACN/0.1% FA for LC-MS/MS.

804 Fractions were analyzed by LC-MS/MS using a NanoAcquity (Waters) with a 50 cm (inner  
805 diameter 75 µm) EASY-Spray Column (PepMap RSLC, C18, 2 µm, 100 Å) heated to 60°C  
806 coupled to an Orbitrap Eclipse Tribrid Mass Spectrometer (Thermo Fisher Scientific). Peptides  
807 were separated by direct injection at a flow rate of 300 nL/min using a gradient of 5 to 30%  
808 acetonitrile (0.1% FA) in water (0.1% FA) over 3 hours and then to 50% ACN in 30 min and  
809 analyzed by SPS-MS3. MS1 scans were acquired over a range of m/z 375-1500, 120K  
810 resolution, AGC target (standard), and maximum IT of 50 ms. MS2 scans were acquired on  
811 MS1 scans of charge 2-7 using isolation of 0.5 m/z, collision-induced dissociation with activation  
812 of 32%, turbo scan, and max IT of 120 ms. MS3 scans were acquired using specific precursor  
813 selection (SPS) of 10 isolation notches, m/z range 110-1000, 50K resolution, AGC target  
814 (custom, 200%), HCD activation of 65%, max IT of 150 ms, and dynamic exclusion of 60 s.

815 **Visualization of translation in TGs**

816 The SunTag system was used to visualize mRNA translation in the cytosol and the TGER  
817 domain. Stable expression of td-PP7-3xmCherry (Addgene 74926) and scFv-GCN4-sfGFP  
818 (Addgene 60907) was achieved by generating virus in HEK293T cells and transducing HeLa  
819 cells. Cells were seeded on 3.5 cm glass bottom dishes (Cellvis, D35-20-1-N). 20 hours later,  
820 cells were transfected with either the SunTag vector expressing KIF18B (Addgene 74928) or  
821 SunTag-FOS-UTR. At 15 hours post transfection, cells were treated with 100 ng/ml doxycycline  
822 for one hour to induce SunTag expression. Confocal imaging was performed as described  
823 above. Colocalization of foci was quantified using FIJI.

#### 824 **mRNA localization-dependent GFP protein expression**

825 Transfection. HeLa cells were seeded in 12-well plates at 80% confluence and transfected with  
826 250 ng GFP-THAP1-MS2 and 250 ng of the MCP-mCherry fusion constructs indicated in the  
827 figure (Lipofectamine 3000, Invitrogen). When indicated, GFP-THAP1 or GFP-BIRC3-MS2-SU  
828 was used instead of GFP-THAP1-MS2. At 13-15 hours post transfection, cells were analyzed by  
829 FACS. For RNA-FISH experiments, cells were seeded at 80% confluence in 4-well slide  
830 chambers (Millipore Sigma) and cotransfected with 75 ng GFP-THAP1-MS2, 100 ng BFP-  
831 SEC61B, and 75 ng of the indicated MCP-mCherry fusion constructs.

832 FACS analysis to measure GFP protein expression. Cells were trypsinized, washed once in  
833 complete media, then resuspended in FACS buffer (PBS plus 1% FCS). At least 5,000 cells  
834 were measured on a BD LSR-Fortessa Cell Analyzer and FACS data were analyzed using  
835 FlowJo software. GFP protein expression corresponds to GFP mean fluorescence intensity  
836 (MFI). To determine the effect of MCP-tethered RBPs on protein output of the GFP reporter  
837 mRNA, only cells that were successfully cotransfected with both the MCP-mCherry fusion and  
838 the GFP reporter constructs were analyzed. To do so, the double-positive cells  
839 (mCherry+/GFP+) were gated, and all single positive and unstained cells were excluded from  
840 the analysis. The reported GFP MFI was calculated from the double-positive cells.  
841 Untransfected cells were used to draw the gates for mCherry+ or GFP+ cells.

842 qPCR analysis to measure GFP mRNA abundance. Cells were trypsinized, washed once in  
843 complete media, then resuspended in FACS buffer (PBS plus 1% FCS). To determine the effect  
844 of MCP-tethered RBPs on GFP reporter mRNA stability, cells were sorted based on expression  
845 of both the MCP-mCherry fusion and the GFP reporter constructs. The BD FACSAria III cell  
846 sorter was used to collect 50,000 cells from each co-transfected population. Cells were sorted  
847 directly into 1 ml of TRIzol solution in Eppendorf tubes for total RNA was extraction. cDNA  
848 synthesis was performed on 200 ng of RNA per sample using the SuperScript IV VILO ezDNase  
849 Master Mix (Invitrogen). ezDNase enzyme was included to eliminate plasmid DNA  
850 contamination. To measure the relative expression levels of reporter mRNA by qRT-PCR,  
851 FastStart Universal SYBR Green Master Mix (ROX) from Roche was used together with GFP-  
852 qPCR F/R primers. GAPDH was used as a housekeeping gene.

853

854

#### 855 **Data analysis**

#### 856 **RNA-seq of subcytoplasmic fractions from HEK293T cells**

857 RNA-seq. Alignment was generated in Dragen v3.10 (Illumina) against the hg38-alt-masked-v2  
858 reference acquired from GENCODE v43 with default parameters. Gene expression analysis  
859 was performed using HOMER v4.11 software.<sup>60</sup> The mean RPKM values of all biological  
860 replicates were calculated and used for downstream analyses. Only protein-coding genes were  
861 analyzed. A gene was considered expressed if the RPKM value is 3 or greater.

862 Classification of membrane/secretory proteins versus non-membrane proteins. Information on  
863 the presence of transmembrane domains or a signal sequence was obtained from uniprot. All  
864 expressed genes were separated into mRNAs that encode membrane/secretory proteins or  
865 non-membrane proteins. If a protein contains a signal sequence but not a transmembrane  
866 domain, it is considered as secretory protein. All proteins with transmembrane domains are  
867 considered membrane proteins and all remaining proteins are classified as non-membrane  
868 proteins. Among the 9155 mRNAs expressed in HEK293T cells, 2140 were classified as  
869 membrane/secretory proteins, whereas 7015 were classified as non-membrane proteins (Table  
870 S1).

871 Compartment-specific localization scores. The sum of RPKM values obtained from TG particles,  
872 ER particles, and the cytosol was considered as total cytoplasmic mRNA expression. For each  
873 gene, the mean compartment-specific RPKM value was divided by the total cytoplasmic mRNA  
874 expression. As a result, each gene is assigned three localization scores that correspond to the  
875 fraction of its transcripts that localize to each of the three compartments: TGs, the ER, and the  
876 cytosol.

877 Compartment-specific enrichment of mRNAs that encode membrane/secretory proteins. We  
878 considered an mRNA to be ER-enriched if the ratio of localization scores (ER/TG) was greater  
879 than 1.25 and classified it as TG-enriched if it was smaller than 0.8. The median localization  
880 score of membrane/secretory mRNAs in the cytosol was 0.09. If the cytosolic localization score  
881 of an mRNA was greater than 0.36, it was considered enriched in the cytosol. If the ER and TG-  
882 specific localization scores were similar and the cytosolic partition coefficient was smaller than  
883 0.18, the mRNA was assigned to the ER, whereas it was considered not localized if the  
884 cytosolic localization score was smaller than 0.18 (Fig. S1H).

885 Compartment-specific enrichment of mRNAs that encode non-membrane proteins. To faithfully  
886 compare differences in mRNA distribution across the three compartments, it is necessary to  
887 know the relative size distribution of the three compartments. However, this parameter is  
888 currently unknown. Therefore, instead of comparing the localization scores across samples, we  
889 determined the most enriched mRNAs within each compartment. We considered an mRNA  
890 compartment-enriched, if its average localization score (from biological replicates) was at least  
891 1.25-fold higher than the median localization score of its corresponding compartment samples.  
892 For TG particles, the median localization score was 0.32, for ER particles, it was 0.30, and for  
893 the cytosol, the median localization score was 0.34. If the enrichment was observed in two  
894 compartments, the mRNA was assigned to the compartment with the higher value. With this  
895 strategy, we identified 1246 TG+ mRNAs, 919 non-overlapping ER+ mRNAs, and 1481 CY+  
896 mRNAs. The remaining 3369 mRNAs (48%) do not have a compartment-biased mRNA  
897 localization pattern and were called (unbiased).

898 Justification of the cut-off used to determine compartment-enriched mRNAs. A minimum cut-off  
899 of 1.25-fold higher than the median localization score corresponds to approximately one  
900 standard deviation. The compartment-enriched mRNAs differed substantially in their functional  
901 and architectural features (Fig. 2). We generated subgroups among the compartment-enriched  
902 mRNAs that represent the top, middle, and bottom-enriched subgroups (Fig. S4). Even when  
903 focusing on the bottom-enriched groups (which are close to the cut-off used), the differences in  
904 functional and architectural features across the compartment-enriched groups were still highly  
905 significant (Fig. S4). The cut-off is further justified as we were able to validate 10/11 mRNAs  
906 considered to be compartment enriched with an independent method. Moreover, we  
907 demonstrate that TG-translated MYC has biological effects, despite MYC mRNA being found in  
908 the bottom enriched TG+ group.<sup>19</sup>

909 **mRNA transcript distribution in HEK293T TIS11B KO cells**

910 We focused on the analysis of mRNAs that encode non-membrane proteins (Table S5). The  
911 mean RPKM values of the biological replicates of digitonin-extracted samples and the ER  
912 particles were calculated for TIS11B KO cells and their corresponding control HEK293T cells. A  
913 gene was considered expressed if the average RPKM value in the ER and in the cytosol  
914 samples was greater than 3 RPKM ( $N = 6229$ ). The compartment-specific localization scores  
915 were calculated and the difference in localization scores between TIS11B KO and control  
916 samples were calculated for ER and cytosol. The top 20% of genes with a localization change  
917 towards ER or the cytosol were intersected with genes considered as TG+ ( $N = 1246$ ) and  
918 further analyzed with respect to their bound RBPs and architectural features.

919 **mRNA and protein features of the localized mRNAs**

920 RPKM values of mRNAs were obtained from RNA-seq data of unfractionated HEK293T cells  
921 and were determined for the compartment-biased mRNAs. Pro-seq and RNA-seq from HEK293  
922 cells were obtained from GEO (GSE140365: PRO-seq; GSE142895: RNA-seq).<sup>27</sup> Raw reads  
923 were processed by trimmomatic (version: 0.39) to trim low-quality ends (average quality per  
924 base < 15, 4 bp window) and adapters.<sup>61</sup> Trimmed reads were mapped to the human genome  
925 (hg19) using hisat2 (version: 2.1.0).<sup>62</sup> Reads mapped to each gene were counted by  
926 featureCounts (version: 1.6.4).<sup>63</sup> To estimate mRNA stability rates, log2-normalized counts of  
927 Pro-seq data were divided by the log2-normalized RNA-seq data, as described previously<sup>28</sup>.  
928 3'UTR length of each mRNA was obtained from Ref-seq. The longest 3'UTR isoform of each  
929 gene is reported. mRNA length, CDS length, average CDS exon length, and total exon number  
930 of genes were determined using transcripts from the Matched Annotation from  
931 the NCBI and EMBL-EBI (MANE)<sup>64</sup> human version 1.2. For each gene, the transcript with  
932 longest mRNA length was selected. Protein length was calculated by dividing CDS length by  
933 three.

934 **Proteomics protein expression analysis**

935 Protein expression was obtained from TMT-based quantitative mass spectrometry analysis of  
936 HEK293T cells. Precursor protein abundance was calculated for each protein and scaled to the  
937 TMT abundance for each channel. Relative abundance was then calculated by averaging the  
938 condition-specific biological replicates. In brief, mass spectra were processed using Protein  
939 Discoverer 2.5 (ThermoFisher) using the Minora algorithm (set to default parameters) for  
940 precursor quantification and using a TMTpro workflow for TMT-based quantification. Database  
941 searching included all canonical entries from the human Reference Proteome UniProt database  
942 (SwissProt – 2022-03), as well as an in-house curated list of contaminants. The identification of  
943 proteins was performed using the SEQUEST-HT engine against the database using the  
944 following parameters: a tolerance level of 10 ppm for MS<sup>1</sup> and 0.6 Da for MS<sup>2</sup> post-recalibration  
945 and the false discovery rate of the Percolator decoy database search was set to 1%. Trypsin  
946 was used as the digestion enzyme, two missed cleavages were allowed, and the minimal  
947 peptide length was set to 7 amino acids. Carbamidomethylation of cysteine residues (+57.021  
948 Da) was set as static modifications, while oxidation of methionine residues (+15.995 Da) was  
949 set as a variable modification. The final protein-level FDR was set to 1%. Precursor abundance  
950 quantification was determined based on intensity, and the minimum replicate feature parameter  
951 was set at 50%. Proteins were quantified based on unique and razor peptides and proteins with  
952 less than two different peptides were excluded. For TMT-based quantification, similar search  
953 parameters were used, with the addition of TMTpro tags on lysine residues and peptide N  
954 termini (+304.207 Da) set as static modifications. For TMTpro-based reporter ion quantitation,  
955 the summed signal-to-noise (S:N) ratio for each TMT channel was extracted, and the closest  
956 matching centroid to the expected mass of the TMT reporter ion was found (integration  
957 tolerance of 0.003 Da). PSMs with poor quality, MS<sup>3</sup> spectra with TMT reporter ion channels  
958 missing, or isolation specificity less than 0.7, or with less than 70% of SPS masses matching to

959 the identified peptides, or with an average TMT reporter summed signal-to-noise ratio that was  
960 less than 10 or had no MS<sup>3</sup> spectra were excluded from quantification. We exported the results  
961 of protein identification and quantification to Excel, including the TMT-based reporter ion  
962 quantitation. Additionally, we extracted the MS<sup>1</sup> precursor abundance for each protein (Minora  
963 algorithm), which indicates its relative abundance in the tryptic sample. Each MS<sup>1</sup>-based  
964 abundance measured should be a representation of the sum of all the respective TMT-labeled  
965 peptides combined. Therefore, for a rudimentary metric of protein abundance across samples,  
966 we divided the total MS<sup>1</sup>-abundance for individual proteins by their respective TMT summed  
967 signal-to-noise ratio to each TMT channel.

968 **CLIP data analysis**

969 **iCLIP analysis of TIS11B in HEK293T cells.** Raw fastq files were demultiplexed using the iCount  
970 python package (<https://icount.readthedocs.io>). 5' and 3' adapters were trimmed by Cutadapt.<sup>65</sup>  
971 Trimmed reads were mapped to human genome using STAR and reads mapping to tRNA/rRNA  
972 were discarded.<sup>66</sup> Crosslink sites were called from bam files using the "xlsites" function of  
973 iCount. CLIP-seq analysis was carried out on the iMaps platform  
<https://imaps.genialis.com/iclip>), where peak calling was performed by analysing cDNA counts  
974 at crosslink sites using Paraclu.<sup>67</sup> Motif analysis was carried out using HOMER software.  
975 Enrichment was calculated within the genomic coordinates of a total of 57,714 TIS11B CLIP  
976 peaks found in 3'UTRs. Total peaks: 190,920; peaks in 3'UTRs: 57,714.

977 **POSTAR3 CLIP data.** CLIP data on 168 RBPs were downloaded from Postar3<sup>34</sup> and peak  
978 counts that overlapped with annotated 3'UTRs from Ref-seq in all mRNAs that encode non-  
979 membrane proteins were recorded. For each RBP, the median number of 3'UTRs CLIP peaks  
980 was calculated and all 3'UTRs with peaks counts greater than the median were considered as  
981 targets. Based on the fraction of mRNAs that are considered compartment-specific (TG: 17.8%;  
982 ER 13.1%; CY: 21.1%; unbiased: 48.0%), we determined the expected number of target genes  
983 for each compartment. If the observed number of targets divided by the expected number of  
984 targets in a compartment was greater than 1.5, the RBP was added to our short-list (Table S4).  
985 As TIS11B and TIA1/L1 are known to bind to AU-rich sequences, we added the processed  
986 PAR-CLIP data of the LARP4B RBP as it was reported to bind to AU-rich elements.<sup>33</sup>

987 **Logistic regression.** The R package `nnet` (v7.3-17) was used to fit logistic regression models to  
988 predict the subcytoplasmic mRNA localization of non-membrane proteins. An initial model used  
989 CLIP peak counts from the RBPs on the short list ( $N = 24$ ). A second model used the top seven  
990 RBPs from the first model fit and added mRNA length and average CDS exon length.  
991 Covariates with missing values were imputed as zeros. All covariates were first `sqrt`  
992 transformed and then standardized. The 'unbiased' category was used as the base level. The R  
993 package `broom` (v0.8.0) was used to compute t-test statistics for the model coefficients. The  
994 code is available on github ([github.com/Mayrlab/tiger-seq](https://github.com/Mayrlab/tiger-seq)).

995 **Confirmation of the logistic regression.** To validate the contribution of each individual RBP, we  
996 used more stringent criteria to determine their targets. Among all mRNAs that encode non-  
997 membrane proteins with at least one CLIP peak in the 3'UTR, we considered the top third of  
998 mRNAs as targets of each RBP (TIS11B: 1781 targets; TIA1/L1: 1313 targets; LARP4B: 1621  
1000 targets; METAP2: 256 targets; HuR: 1124 targets; PUM2: 427 targets; HNRNPC: 232 targets).  
1001 mRNAs only bound by LARP4B or METAP2 are LARP4B/METAP2 targets and not bound by  
1002 another RBP (from the seven RBPs investigated),  $N = 717$ . mRNAs predominantly bound by  
1003 TIS11B are TIS11B targets exclusively bound by TIS11B or co-bound by TIA1/L1, with  
1004 TIS11B/TIA1/L1  $\geq 2$  ( $N = 834$ ). mRNAs predominantly bound by TIA1/L1 are TIA1/L1 targets  
1005 exclusively bound by TIA1/L1 or co-bound by TIS11B but TIS11B/TIA1/L1  $< 2$  ( $N = 634$ ).

1006 **Intersection of membrane/secretory mRNAs with previous datasets.** APEX-seq. The  
1007 mRNAs that are coexpressed in our RNA-seq dataset ( $N = 9155$  mRNAs) and the ER  
1008 membrane-localized mRNAs from the APEX-seq dataset ( $N = 1045$ ) were determined.<sup>11</sup> The  
1009 overlapping 845 mRNAs were intersected with the mRNAs that encode membrane/secretory  
1010 proteins found to be ER+ in our analysis ( $N = 1476$ ). We detected 673 mRNAs which  
1011 correspond to 80% of all APEX-seq mRNAs that are considered to be ER membrane (ERM)-  
1012 enriched. The universe used to test for enrichment were all mRNAs that encode non-membrane  
1013 proteins ( $N = 2140$ ). **Biochemical fractionation.** A similar analysis was performed for the  
1014 fractionation dataset from Reid (2012).<sup>9</sup> Among the 385 coexpressed mRNAs that are enriched  
1015 on the ER according to Reid, we detected 308 in our ER+ fraction when focusing on  
1016 membrane/secretory protein encoding mRNAs. This group represents 80% of all ER-enriched  
1017 mRNAs detected by Reid. **MERFISH.** In the MERFISH dataset, which was generated in U2OS  
1018 cells, 1037 mRNAs are considered ER-enriched. Among them,  $N = 571$  are co-expressed in our  
1019 dataset and considered mRNAs encoding membrane/secretory proteins. Among the 571 co-  
1020 expressed mRNAs we consider 511 as ER+, which corresponds to 89%. Among the ER-de-  
1021 enriched mRNAs (Log2FC nonER vs ER = -0.34), only 69 mRNAs encode membrane/secretory  
1022 proteins. Among the 69 mRNAs, we consider 8 as ER+, which corresponds to 11.6%.<sup>13</sup>

1023 **Intersection of mRNAs that encode non-membrane proteins with a previous dataset.** The  
1024 relative distribution of mRNA transcripts across subcellular compartments, including the  
1025 membrane fraction, phase-separated granules, and the cytosol was determined using density  
1026 gradient centrifugation in U2OS cells.<sup>25</sup> The number of co-expressed mRNAs that encode non-  
1027 membrane proteins was  $N = 6557$ , which corresponds to 93% of our dataset. This dataset  
1028 determines the proportion of transcripts that localize to the different fractions. For co-expressed  
1029 TG+ mRNAs ( $N = 1153$ ), ER+ mRNAs ( $N = 839$ ) and CY+ mRNAs ( $N = 1400$ ), we plotted the  
1030 proportion of mRNAs that localize to phase-separated granules, to the membrane fraction, and  
1031 to the cytosol in the LoRNA dataset in U2OS cells.

### 1032 **Gene ontology analysis**

1033 Gene ontology (GO) analysis was performed using DAVID.<sup>30</sup>

### 1034 **Further statistical analysis**

1035 Statistical parameters are reported in the figures and figure legends, including the definitions  
1036 and exact values of  $N$  and experimental measures (mean  $\pm$  std or boxplots depicting median,  
1037 25<sup>th</sup> and 75<sup>th</sup> percentile (boxes) and 5% and 95% confidence intervals (error bars)). Pair-wise  
1038 transcriptomic feature comparisons were performed using a two-sided Mann-Whitney test. For  
1039 more than two samples, a Kruskal-Wallis test was performed. For transcriptomic analyses,  
1040 statistical significance is indicated by asterisks \*,  $0.05 > P > 1 \times 10^{-9}$ ; \*\*,  $1 \times 10^{-10} > P > 1 \times 10^{-20}$ ;  
1041 \*\*\*,  $1 \times 10^{-21} > P > 1 \times 10^{-80}$ ; \*\*\*\*,  $1 \times 10^{-81} > P > 0$ . Exact  $P$  values are listed in Table S3.  
1042 Enrichment was determined using a  $\chi^2$  test. The  $P$  value was calculated using a two-sided  
1043 Fisher's exact test. When indicated, a two-sided t-test with assumption of equal variance was  
1044 applied. Statistical significance for experimental data is indicated by asterisks \*,  $P < 0.05$ , \*\*,  $P <$   
1045 0.01, \*\*\*,  $P < 0.001$ , \*\*\*\*,  $P < 0.0001$ .

### 1046 **Data and code availability**

1047 The data of the proteomics experiment were deposited in the MassIVE repository (dataset  
1048 identifier MSV000092176). The RNA-seq samples obtained from the subcytoplasmic  
1049 fractionation and the TIS11B iCLIP data obtained from HEK293T cells are available at GEO  
1050 (Accession number: GSE215770). The code for logistic regression is available on github  
1051 ([github.com/Mayrlab/tiger-seq](https://github.com/Mayrlab/tiger-seq)). Raw western blot data, raw imaging data and scripts for  
1052 analysis are deposited at Mendeley (<https://data.mendeley.com/datasets/nmt7ppsp8r/1>).

1053 **Figure Legends**

1054 **Figure 1. Strategy to identify compartment-enriched mRNAs.**

1055 1A. Confocal live cell imaging of HeLa cells after transfection of mCherry (mC)-TIS11B and  
1056 GFP-SEC61B to visualize TGs and the rough ER. Scale bar, 5  $\mu$ m.

1057 1B. Schematic of a cell with three cytoplasmic compartments.

1058 1C. As in (A) but showing fluorescent TG (left) and ER (right) particles. Scale bar, 5  $\mu$ m.

1059 1D. The transcript localization scores for the TG samples are shown for all mRNAs that encode  
1060 non-membrane proteins ( $N = 7015$ ), for the mRNAs defined as TG+ ( $N = 1246$ ), and for mRNAs  
1061 considered to have an unbiased transcript distribution ( $N = 3369$ ) to illustrate that the relative  
1062 transcript distribution between TG+ and unbiased mRNAs is substantially different. Mann  
1063 Whitney test,  $P = 0$ .

1064 1E. As in (D), but the transcript localization scores for the ER samples are shown for all mRNAs  
1065 that encode non-membrane proteins ( $N = 7015$ ), for the mRNAs defined as ER+ ( $N = 919$ ), and  
1066 for mRNAs considered to have an unbiased transcript distribution ( $N = 3369$ ). Mann Whitney  
1067 test,  $P = 1 \times 10^{-123}$ .

1068 1F. As in (D), but the transcript localization scores for the cytosolic fractions are shown for all  
1069 mRNAs that encode non-membrane proteins ( $N = 7015$ ), for the mRNAs defined as CY+ ( $N =$   
1070 1481), and for mRNAs considered to have an unbiased transcript distribution ( $N = 3369$ ). Mann  
1071 Whitney test,  $P = 0$ .

1072 1G. SmRNA-FISH of endogenous TG+ mRNA *BAG3* (green) in HeLa cells. TIS granules (BFP-  
1073 TIS11B, blue) and the ER (GFP-SEC-61B, magenta) were simultaneously visualized. Bottom  
1074 panel shows a 5x zoom-in of the area indicated by dashed white box. White circles indicate  
1075 colocalization of mRNA puncta with TGs, whereas dashed white circles indicate colocalization  
1076 with the ER. Representative images are shown. Scale bar, 5  $\mu$ m.

1077 1H. As in (G), but smRNA-FISH of the endogenous ER+ mRNA *ALDH18A1* is shown.

1078 1I. Quantification of TG-localizing smRNA-FISH foci of three TG+ and five ER+ endogenous  
1079 mRNAs. The white box plot indicates the expected fraction of mRNA transcripts based on the  
1080 TG compartment size, obtained from of 186 cells. mRNAs defined as TG+ are enriched in TGs  
1081 (Mann Whitney test, \*\*\*, (TG),  $P = 5 \times 10^{-11}$ ), whereas mRNAs defined as ER+ are not enriched.  
1082 Additional images are shown in Fig. S2A-F and values for the individual mRNAs are shown in  
1083 Fig. S2H.

1084 1J. As in (I) but quantification of ER-localizing smRNA-FISH foci of three TG+ and five ER+  
1085 endogenous mRNAs. The white box plot indicates the expected fraction of mRNA transcripts  
1086 based on the ER compartment size, obtained from of 186 cells. mRNAs defined as ER+ are  
1087 enriched on the ER (Mann Whitney test, \*\*\*, (TG),  $P = 1 \times 10^{-6}$ ), whereas mRNAs defined as  
1088 TG+ are not enriched. Values for the individual mRNAs are shown in Fig. S2I.

1089 1K. The ratio of smRNA-FISH foci colocalizing with the ER compared to the foci colocalizing  
1090 with TGs is shown for the TG+ and ER+ endogenous mRNAs from (I) and (J). T-test for  
1091 independent samples, \*,  $P = 0.044$ .

1092 1L. smRNA-FISH foci of endogenous mRNAs in HeLa cells before (-) and after (+) digitonin  
1093 extraction. Cell boundaries are indicated by the dotted lines. Representative images are shown.  
1094 Scale bar, 5  $\mu$ m.

1095 1M. Quantification of (L). Shown is the fraction of digitonin-resistant smRNA-FISH foci of  
1096 endogenous mRNAs as mean  $\pm$  std of three independent experiments. Number of cells

1097 analyzed, *MLST8*,  $N = 70$ ; *SF3A2*,  $N = 67$ ; *MAP2K2*,  $N = 48$ ; *ALDH18A1*,  $N = 63$ ; *TES*,  $N = 81$ ;  
1098 *IDH*,  $N = 127$ ; *BAG3*,  $N = 187$ ; *DUSP1*,  $N = 162$ ; *DNAJB1*,  $N = 138$ . Additional images are  
1099 shown in Fig. S3A-C. T-test for independent samples, \*,  $P < 0.041$ .

1100 1N. Summary of the smRNA-FISH validation for mRNAs defined as compartment enriched.  
1101

1102 **Figure 2. Characteristics of compartment-enriched mRNAs.**

1103 2A. Steady-state mRNA abundance levels obtained from whole cell lysates. TG+,  $N = 1246$ ;  
1104 ER+,  $N = 919$ , CY+,  $N = 1481$ ; unbiased,  $N = 3369$ . Mann Whitney test: \*,  $0.05 > P > 1 \times 10^{-9}$ ; \*\*,  
1105  $1 \times 10^{-10} > P > 1 \times 10^{-20}$ ; \*\*\*,  $1 \times 10^{-21} > P > 1 \times 10^{-80}$ ; \*\*\*\*,  $1 \times 10^{-81} > P > 0$ . Exact  $P$  values are listed  
1106 in Table S3. RPKM, reads per kilobase of transcript per million reads mapped.

1107 2B. As in (A), but steady-state protein levels obtained from whole cell lysates are shown. TG+,  
1108  $N = 469$ ; ER+,  $N = 638$ ; CY+,  $N = 833$ ; unbiased,  $N = 2001$ .

1109 2C. As in (B), but Pro-seq levels are shown, which indicate transcription rates. TG+,  $N = 1222$ ;  
1110 ER+,  $N = 896$ ; CY+,  $N = 1425$ ; unbiased,  $N = 3268$ .

1111 2D. As in (C), but estimated mRNA half-lives are shown.

1112 2E. As in (A), but protein size distributions are shown. AA, amino acid

1113 2F. As in (A), but mRNA length distributions are shown.

1114 2G. As in (A), but 3'UTR length distributions are shown.

1115 2H. As in (A), but average CDS exon length distributions are shown.

1116 2I. Gene model of *ZFP36L1* (TIS11B) showing its unusual CDS exon length distribution. Tall  
1117 boxes indicate CDS exons and the narrow boxes indicate the 5' and 3'UTRs.

1118 2J. Gene ontology analysis for TG+ mRNAs. Shown are the top six functional gene classes and  
1119 their Benjamini-Hochberg adjusted  $P$  values for categories that are significantly and uniquely  
1120 enriched in TG+ mRNAs. The Benjamini-Hochberg adjusted  $P$  values for the same categories  
1121 for ER+ and CY+ mRNAs are shown for comparison.

1122 2K. As in (J), but for ER+ mRNAs.

1123 2L. As in (J), but for CY+ mRNAs.

1124

1125 **Figure 3. mRNA architecture features together with RBPs determine the subcytoplasmic  
1126 transcript distribution.**

1127 3A. 3'UTR-bound RBPs that are positively or negatively associated with compartment-enriched  
1128 mRNAs. Shown are the -log10 transformed  $P$  values obtained from logistic regression (see  
1129 Table S4).

1130 3B. Pearson's correlation coefficients of mRNA and exon length with compartment localization  
1131 scores (LS).

1132 3C. As in (A) but integrating 3'UTR-bound RBPs from (A) and the mRNA architecture features  
1133 'mRNA length' and 'CDS exon length'.

1134 3D. The propensity to localize to TGs is shown for mRNAs stratified by exon length and bound  
1135 RBPs. No RBP ( $N = 1498$ ), bound only by LARP4B or METAP2 ( $N = 717$ ) or only by TIS11B ( $N$   
1136 = 834). Mann Whitney test was performed.  $P$  value categories as in Fig. 2A.

1137 3E. Model showing the additive effects of exon length and RBPs on the mRNA localization  
1138 propensity to TGs or the cytosol. RBPs can have positive (check) or negative (x) effects. Shown  
1139 as in Fig. 2I.

1140 3F. As in (D) but shown is the propensity of mRNAs to localize to the ER, stratified by mRNA  
1141 length and the bound RBPs. Bound only by TIA1/L1 ( $N = 634$ ).

1142 3G. As in (E) but showing the additive effects of mRNA length and RBPs on the mRNA  
1143 localization propensity to the ER or the cytosol. RBPs can have positive or negative effects.

1144 3H. As in (F) but shown is the propensity of mRNAs to localize to the cytosol. mRNAs bound  
1145 only by LARP4B or METAP2 ( $N = 717$ ) or only by TIS11B ( $N = 834$ ).

1146

1147 **Figure 4. Experimental validation of the regulators of subcytoplasmic mRNA transcript**  
1148 **distribution.**

1149 4A. TG+ mRNAs are shown and are color-coded based on their change in compartment  
1150 localization in TIS11B KO cells compared with control cells. No change ( $N = 508$ ); up in the ER  
1151 ( $N = 197$ ); up in CY ( $N = 217$ ).

1152 4B. Length distribution of mRNAs from (A). Mann Whitney test was performed.  $P$  value  
1153 categories as in Fig. 2A. Exact  $P$  values are listed in Table S3.

1154 4C. As in (B) but shown is protein size distribution.

1155 4D. As in (B) but shown is CDS exon length distribution.

1156 4E. As in Fig. 3E but shown are the mRNA features of TG+ mRNAs that change their  
1157 localization upon TIS11B KO.

1158 4F. Schematic of the mRNA reporter used to validate the effect of a single 3'UTR-bound RBP  
1159 on mRNA localization. The *GFP-THAP1* reporter mRNA contains MS2 hairpins as 3'UTR, which  
1160 allow binding of the cotransfected MS2 coat protein (mCherry-tagged MCP). Fusion of TIAL1 to  
1161 MCP tethers it to the 3'UTR of the reporter mRNA. mC, mCherry.

1162 4G. Confocal live cell imaging of HeLa cells expressing the indicated constructs. Scale bar, 5  
1163  $\mu\text{m}$ .

1164 4H. RNA-FISH (teal) of the GFP reporter mRNA from (F) in HeLa cells coexpressing the  
1165 indicated MCP-fusion construct together with BFP-SEC61B to visualize the rough ER  
1166 (magenta). Representative confocal images are shown. Scale bar, 5  $\mu\text{m}$ .

1167 4I. Line profiles of the fluorescence intensities obtained from the arrows shown in (H) together  
1168 with the obtained Pearson's correlation coefficients.

1169 4J. Quantification of the Pearson's correlation coefficients between the *GFP-THAP1* reporter  
1170 mRNA and the rough ER in the experiment shown in (H). Two line profiles were generated for  
1171 each cell. For MCP,  $N = 26$  cells and for MCP-TIAL1  $N = 21$  were analyzed. The horizontal line  
1172 denotes the median and the error bars denote the 25<sup>th</sup> and 75<sup>th</sup> percentiles. Mann-Whitney test,  
1173 \*\*\*,  $P < 0.0001$ .

1174

1175 **Figure 5. 3'UTR-bound TIAL1 cooperates with the rough ER membrane environment to**  
1176 **increase protein expression.**

1177 5A. Protein abundance of mRNAs stratified by RBP binding. No RBP ( $N = 126$ ), bound only by  
1178 TIS11B ( $N = 267$ ), bound only by TIA1/L1 ( $N = 232$ ). Mann Whitney test was performed.  $P$  value  
1179 categories as in Fig. 2A.

1180 5B. GFP protein expression measured by FACS in HeLa cells using the *GFP-THAP1* reporter  
1181 mRNA with and without TIAL1 tethering. Representative histograms are shown. GFP-negative  
1182 cell populations are shown as dotted lines.

1183 5C. Quantification of the experiment shown in (B). Shown is the mean  $\pm$  std of five independent  
1184 experiments. T-test for independent samples, \*\*\*\*,  $P = 0.0003$ .

1185 5D. Quantification of mRNA level of the experiment from (B). Shown is the mean  $\pm$  std of three  
1186 independent experiments. T-test for independent samples, NS, not significant.

1187 5E. Schematic of a *GFP-THAP1* mRNA reporter that investigates the influence of subcellular  
1188 mRNA localization on protein expression. Fusion of MCP to SEC61B localizes the GFP reporter  
1189 mRNA (shown as in Fig. 4F) to the rough ER membrane, whereas MCP alone localizes it to the  
1190 cytosol.

1191 5F. Confocal live cell imaging of HeLa cells expressing the indicated constructs. Scale bar, 5  
1192  $\mu\text{m}$ .

1193 5G. As in (B) but the *GFP-THAP1* reporter mRNA was used with and without SEC61B tethering.

1194 5H. Quantification of the experiment from (G). Shown is the mean  $\pm$  std of four independent  
1195 experiments. T-test for independent samples, \*\*,  $P = 0.0026$ .

1196 5I. Quantification of mRNA level in the experiment from (G). Shown is the mean  $\pm$  std of three  
1197 independent experiments. T-test for independent samples, NS, not significant.

1198 5J. As in Fig. 4F, but addition of a prenylation signal (CAAX) localizes the TIAL1-bound *GFP-*  
1199 *THAP1* reporter mRNA to the plasma membrane. In the absence of CAAX, the TIAL1-bound  
1200 reporter mRNA localizes to the rough ER.

1201 5K. Confocal live cell imaging of HeLa cells expressing the indicated constructs. Scale bar, 5  
1202  $\mu\text{m}$ .

1203 5L. As in (B) but the *GFP-THAP1* reporter mRNA was tethered with the indicated constructs.

1204 5M. Quantification of the experiment from (L). Shown is the mean  $\pm$  std of four independent  
1205 experiments. T-test for independent samples, \*\*\*\*,  $P < 0.0006$ , \*\*,  $P = 0.002$ .

1206 5N. Endogenous mRNAs bound by TIA1/L1 encode higher expressed proteins than mRNAs not  
1207 bound by any RBP. The largest TIA1/L1-associated increase was observed for ER+ mRNAs.  
1208 Mann Whitney test was performed.  $P$  value categories as in Fig. 2A.

1209

1210 **Figure 6. Localization of cytosolic mRNAs to the rough ER membrane increases their**  
1211 **protein expression.**

1212 6A. Schematic of a *GFP-THAP1* reporter mRNA bound by TIS11B that allows investigation of  
1213 localization-dependent GFP protein expression. Fusion of MCP and TIS11B localizes the mRNA  
1214 reporter to the cytosol, whereas the TIS11B-MCP-SEC61B fusion localizes the mRNA to the  
1215 rough ER membrane.

1216 6B. Confocal live cell imaging of HeLa cells expressing the constructs from (A). Scale bar, 5  $\mu\text{m}$ .

1217 6C. As in Fig. 5B, but the *GFP-THAP1* reporter mRNA was tethered with the indicated MCP-  
1218 fusion constructs.

1219 6D. Quantification of the experiment from (C). Shown is the mean  $\pm$  std of four independent  
1220 experiments. T-test for independent samples, \*\*\*\*,  $P < 0.0001$ , \*\*,  $P = 0.003$ , NS, not significant.

1221 6E. Quantification of mRNA level in the experiment from (C). Shown is the mean  $\pm$  std of three  
1222 independent experiments. T-test for independent samples, \*,  $P = 0.037$ ; NS, not significant.

1223

1224 **Figure 7. Model.**

1225 Model showing features of endogenous mRNAs with biased subcytoplasmic transcript  
1226 distribution. Summarized are also the changes in protein abundance upon relocalization of the  
1227 reporter from the cytosol to the ER (see text for details). The horizontal arrow indicates no  
1228 change.

1229

1230

1231 **Supplementary Figures**

1232 **Figure S1. Strategy to determine subcytoplasmic mRNA localization.**

1233 S1A. Cell fractionation strategy to obtain the cytoplasmic membrane fraction. Transfected  
1234 HEK293T cells were lysed in hypotonic buffer, followed by douncing and differential  
1235 centrifugation at 600 g to pellet nuclei. The supernatant was subsequently spun at 7000 g. The  
1236 pellet contains the cytoplasmic membrane fraction that was used for subsequent fluorescent  
1237 particle sorting.

1238 S1B. FACS plot showing the gating strategy to obtain mCherry-TIS11B+/GFP-SEC61B+ TG  
1239 particles and mCherry-TIS11B-/GFP-SEC61B+ ER particles. The particles were costained with  
1240 DAPI to segregate TG and ER particles from nuclear contamination (DAPI high). The DAPI low  
1241 particles were sorted.

1242 S1C. Immunoblot showing markers used to evaluate the quality of the three compartment  
1243 fractions. WCL is the unfractionated whole cell lysate. CY is the digitonin-extracted cytosol. Pre-  
1244 sort is the membrane-enriched cytoplasmic lysate from which TG and ER particles are sorted,  
1245 which is the final step in (A). 50K TG indicates 50,000 sorted TG particles and 50K ER indicates  
1246 50,000 sorted ER particles. H3 antibody was used as a marker for nuclear components,  
1247 GAPDH was used as marker for cytosolic proteins, and Calnexin and GFP-SEC61B were used  
1248 as ER markers. \*, signal from mCherry-TIS11B.

1249 S1D. Quantification of endogenous TIS11B and mCherry-TIS11B from (C) together with  
1250 additional biological replicates. Shown is the ratio of protein abundance in 50K TG over 50K ER  
1251 as mean  $\pm$  std of three independent experiments.

1252 S1E. As in (D), but quantification of endogenous Calnexin and GFP-SEC61B. Shown is the ratio  
1253 of protein abundance in 50K ER over 50K CY as mean  $\pm$  std of three independent experiments.

1254 S1F. Correlation of log2-transformed RPKM values obtained by RNA-seq for biological  
1255 replicates of subcytoplasmic compartments. The Pearson correlation coefficients are shown.

1256 S1G. Baseline distribution of localization scores across the three investigated cytoplasmic  
1257 compartments is shown separately for mRNAs that encode membrane/secretory proteins and  
1258 mRNAs that encode non-membrane proteins.

1259 S1H. Distribution of localization scores in each fractionation sample for compartment-enriched  
1260 mRNAs that encode membrane/secretory proteins.

1261 S1I. Overlap of ER+ mRNAs that encode membrane/secretory proteins ( $N = 1476$ ) defined by  
1262 us (particle sorting) with previous datasets that used alternative isolation methods. In the APEX-  
1263 seq dataset 78% of ER-localized mRNAs overlap with our ER+ mRNAs. In the fractionation  
1264 dataset, 80.5% of ER-localized mRNAs overlap with our ER+ mRNAs. Among the MERFISH  
1265 ER-localized mRNAs 89% overlap with our ER+ mRNAs and only 11.6% of our ER+ mRNAs  
1266 overlap with the ER-de-enriched mRNAs obtained by MERFISH.  
1267 S1J. ER+ mRNAs that encode membrane/secretory proteins ( $N = 1476$ ) defined by us are  
1268 significantly enriched on the ER membrane (ERM) according to APEX-seq, whereas CY+  
1269 mRNAs that encode membrane/secretory proteins show a significantly lower ERM enrichment.  
1270 Similarly, CY+ mRNAs that encode membrane/secretory proteins have significantly higher  
1271 APEX2 enrichment scores in the cytosol than mRNAs considered ER+ by us. Mann Whitney  
1272 test:  $P < 2 \times 10^{-7}$ .  
1273 S1K. Ternary plot showing compartment-enriched mRNAs. Each dot represents an mRNA that  
1274 is color-coded as in Fig. 1D-F. mRNAs in the center (light grey) are considered to have an  
1275 unbiased transcript distribution.  
1276 S1L. Distribution of localization scores in each fractionation sample for compartment-enriched  
1277 mRNAs that encode non-membrane proteins.  
1278 S1M. Validation of mRNAs that encode non-membrane proteins and are defined as  
1279 compartment-enriched by us in comparison with the LoRNA dataset. Our TG+ mRNAs are  
1280 highest enriched in the mRNAs that LoRNA identifies in the phase-separated granule fraction.  
1281 Our ER+ mRNAs are highest enriched in the mRNAs that LoRNA identifies in the membrane  
1282 fraction. Our CY+ mRNAs are highest enriched in the mRNAs that LoRNA identifies in the  
1283 cytosol. Mann Whitney test was performed. Exact  $P$  values are listed in Table S3.  
1284

1285 **Figure S2. Validation of endogenous TG+ and ER+ mRNAs by smRNA-FISH.**

1286 S2A. SmRNA-FISH of endogenous TG+ mRNA *DUSP1* (green) in HeLa cells. TGs (BFP-  
1287 TIS11B, blue) and the ER (GFP-SEC-61B, magenta) were simultaneously visualized. The  
1288 maximum projection of the fluorescent signals is shown. Bottom panel shows a 5x zoom-in of  
1289 the area indicated by the white dashed box. White circles indicate colocalization of mRNA  
1290 puncta with TGs, whereas dashed circles indicate colocalization with the ER. Representative  
1291 images are shown. Scale bar, 5  $\mu\text{m}$ .  
1292 S2B. As in (A), but smRNA-FISH of endogenous TG+ mRNA *DNAJB1* is shown.  
1293 S2C. As in (A), but smRNA-FISH of endogenous ER+ mRNA *PLA2GA4* is shown.  
1294 S2D. As in (A), but smRNA-FISH of endogenous ER+ mRNA *IDH1* is shown.  
1295 S2E. As in (A), but smRNA-FISH of endogenous ER+ mRNA *TES* is shown.  
1296 S2F. As in (A), but smRNA-FISH of endogenous ER+ mRNA *ACTN4* is shown.  
1297 S2G. As in (E) but shown is a 2x magnification of the area indicated by the white dashed box.  
1298 The image illustrates the high background signal in the nucleus observed when probing for  
1299 endogenous *TES*. For quantification of this mRNA, the noise tolerance value used in the  
1300 puncta-calling function was increased to limit nuclear background noise. The white circles  
1301 indicate nuclear foci that are included in the quantification at this tolerance level. Scale bar, 5  
1302  $\mu\text{m}$ .  
1303 S2H. Colocalization of TGs and smRNA-FISH foci of three TG+ (beige) and five ER+ (blue)  
1304 endogenous mRNAs. The beige box plot indicates the expected fraction of mRNA transcripts

1305 based on the TG compartment size distribution, obtained from 186 cells. Number of cells  
1306 analyzed for RNA-FISH: *BAG3* ( $N = 17$ ), *DUSP1* ( $N = 30$ ), *DNAJB1* ( $N = 25$ ), *PLA2GA4* ( $N =$   
1307 17), *IDH1* ( $N = 18$ ), *ALDH18A1* ( $N = 22$ ), *TES* ( $N = 34$ ), *ACTN4* ( $N = 23$ ). Mann Whitney test  
1308 shows that the mRNA transcript distribution of 3/3 TG+ mRNAs (beige) is significantly higher  
1309 than what would be expected for unbiased mRNAs.  $P$  value categories as in Figure 2A, exact  $P$   
1310 values listed in Table S3.

1311 S2I. As in (H), but colocalization of the ER and smRNA-FISH foci of three TG+ (beige) and five  
1312 ER+ (blue) endogenous mRNAs. The blue box plot indicates the expected fraction of mRNA  
1313 transcripts based on the ER compartment size distribution, obtained from of 186 cells. Mann  
1314 Whitney test shows that the mRNA transcript distribution of 4/5 ER+ mRNAs (blue) is  
1315 significantly higher than what would be expected for unbiased mRNAs.

1316

1317 **Figure S3. Validation of CY+ mRNAs by smRNA-FISH after digitonin extraction.**

1318 S3A. Shown are smRNA-FISH foci of endogenous *SF3A2* mRNA and *MAP2K2* mRNA in HeLa  
1319 cells before (-) and after (+) digitonin extraction. *SF3A2* and *MAP2K2* are considered CY+  
1320 mRNAs. Cell boundaries are indicated by the dotted lines. Representative images are shown.  
1321 Scale bar, 5  $\mu\text{m}$ .

1322 S3B. As in (A), but smRNA-FISH foci of endogenous *TES* mRNA and *IDH1* mRNA are shown,  
1323 which are considered ER+ mRNAs.

1324 S3C. As in (A), but smRNA-FISH foci of endogenous *DUSP1* mRNA and *DNAJB1* mRNA are  
1325 shown, which are considered TG+ mRNAs.

1326 S3D. Schematic of the reporter mRNA used with the SunTag system to measure nascent  
1327 protein synthesis. CDS, coding sequence. The *KIF18B* construct was used previously.<sup>32</sup>

1328 S3E. Confocal imaging of HeLa cells stably expressing SunTag reporter proteins svFc-GFP and  
1329 mCherry-tagged PP7 protein (mC-PP7) co-transfected with two constructs (i) BFP-TIS11B to  
1330 visualize TGs and (ii) SunTag-labeled mRNA encoding KIF18B with PP7-binding sites in the  
1331 3'UTR. The *KIF18B* mRNA is visualized by mC-PP7 binding (teal) whereas the KIF18B protein  
1332 is visualized by svFc-GFP binding (magenta). Foci with co-localization of mRNA and protein  
1333 represent nascent protein synthesis and are indicative of active translation. A representative  
1334 example is shown. The white box indicated area is shown at 6x magnification in the lower panel.  
1335 White arrows indicate actively translating mRNA, yellow arrow indicates non-translating mRNA.  
1336 Scale bar, 5  $\mu\text{m}$  (top panel), 1  $\mu\text{m}$  (bottom panel).

1337 S3F. Quantification of the experiment from (E). Shown are the number of mRNA foci in TGs or  
1338 the cytosol (CY) using the Suntag reporter from (D). Each dot represents a cell.  $N = 24$  cells  
1339 were analyzed.

1340 S3G. As in (F), but shown are the mRNAs that are actively translated in each compartment,  
1341 which were identified by counting the teal and magenta-double positive foci.

1342

1343 **Figure S4. Characteristics of compartment-enriched mRNAs are shown for subgroups.**

1344 S4A. To justify the cut-off used to determine compartment-enriched mRNAs (Fig. 1D-F), we  
1345 show the data from Figure 2 in more detail. Steady-state mRNA abundance levels obtained  
1346 from whole cell lysates is shown for unbiased mRNAs ( $N = 3369$ ), three subgroups of TG+  
1347 mRNAs (top, middle, bottom,  $N = 415$  each); three subgroups of ER+ mRNAs (top, middle,  
1348 bottom,  $N = 306$  each); three subgroups of CY+ mRNAs (top, middle, bottom,  $N = 493$  each).  
1349 Even when focusing on the bottom-enriched groups (which are close to the cut-off used), the

1350 differences across the compartment-enriched groups are still highly significant. Mann Whitney  
1351 tests were performed. *P* value categories as in Fig. 2A. Exact *P* values are shown in Table S3.  
1352 RPKM, reads per kilobase of transcript per million reads mapped.  
1353 S4B. As in (A), but steady-state protein levels obtained from whole cell lysates are shown.  
1354 S4C. As in Fig. 2C, but steady-state mRNA abundance levels of compartment-enriched mRNAs  
1355 obtained by RNA-seq from whole cell lysates of HEK293 cells are shown. This sample was  
1356 used together with the Pro-seq sample to estimate mRNA half-lives.  
1357 S4D. As in (A), but Pro-seq levels are shown.  
1358 S4E. As in (A), but estimated mRNA half-lives are shown.  
1359 S4F. As in (A), but protein size distributions are shown.  
1360 S4G. As in (A), but mRNA length distributions are shown.  
1361 S4H. As in (A), but 3'UTR length distributions are shown.  
1362 S4I. As in (A), but average CDS exon length distributions are shown.  
1363 S4J. As in Fig. 2A, but the number of exons per mRNA is shown.  
1364 S4K. As in (A), but the number of exons per mRNA is shown.  
1365

1366 **Figure S5. Analyses of TIS11B CLIP data and TIS11B KO samples.**

1367 S5A. Gel showing samples used for iCLIP of GFP-tagged TIS11B. The region outlined in red  
1368 was used for iCLIP sample preparation.  
1369 S5B. TIS11B iCLIP tag distribution obtained from HEK293T cells.  
1370 S5C. The top five motifs that were enriched within TIS11B peaks in 3'UTRs compared to all  
1371 nucleotides in 3'UTRs. Shown are *P* values obtained by HOMER.  
1372 S5D. The fraction of mRNAs bound by at least one RBP (from Fig. 3A) for the different groups  
1373 of compartment-enriched mRNAs is shown.  
1374 S5E. Immunoblot of TIS11B in control cells and TIS11B KO HEK293T cells. H3 was used as  
1375 loading control.  
1376 S5F. Correlation of log<sub>2</sub>-transformed RPKM values obtained by RNA-seq for biological  
1377 replicates of sorted ER particles or digitonin-extracted cytosol samples for control and TIS11B  
1378 KO cells. The Pearson correlation coefficients are shown.  
1379

1380 **Figure S6. mRNA localization-dependent protein expression of the GFP reporter.**

1381 S6A. Gating strategy to assess GFP protein expression of the reporter mRNA by FACS. Left  
1382 panel shows the ungated population of HeLa cells coexpressing MCP-mCherry and the *GFP-*  
1383 *THAP1-MS2* reporter, separated by size (forward scatter) and granularity (side scatter). The  
1384 black circle indicates the live cells that were used for subsequent analysis. Middle panel, the  
1385 *GFP-* and mCherry-double positive population was gated to obtain the GFP mean fluorescence  
1386 values (MFI, right panel) which corresponds to the reported GFP protein expression values.  
1387 S6B. As in (A), but HeLa cells coexpressing MCP-mCherry-TIAL1 and the *GFP-THAP1-MS2*  
1388 reporter.

1389 S6C. As in Fig. 4F and 5C, but the MS2 sites in the GFP reporter were omitted. Top:  
1390 coexpression of MCP-mCherry-TIAL1 does not result in the binding of MCP to the reporter  
1391 mRNA without MS2 sites. This experiment serves as control for the effect of TIA1L1  
1392 overexpression on reporter mRNA expression. Bottom: Quantification of the experiment with the  
1393 GFP mRNA reporter lacking the MS2 binding sites. Shown is the mean  $\pm$  std of three  
1394 independent experiments. T-test for independent samples, NS, not significant.

1395 S6D. Schematic of a second mRNA reporter used to validate the effect of a single 3'UTR-bound  
1396 RBP on protein expression. The *GFP-BIRC3* reporter mRNA contains the BIRC3 coding region  
1397 and MS2 hairpins as 3'UTR, which allow binding of the co-transfected MS2 coat protein  
1398 (mCherry-tagged MCP). Fusion of TIAL1 to MCP tethers TIAL1 to the 3'UTR of the reporter  
1399 mRNA. mC, mCherry.

1400 S6E. GFP protein expression of the reporter mRNA from (D) in HeLa cells, coexpressing the  
1401 indicated MCP-fusion constructs, measured by FACS. Representative histograms are shown.  
1402 GFP-negative cell populations are shown as dotted lines.

1403 S6F. Quantification of the experiment shown in (E). Shown is the mean  $\pm$  std of five  
1404 independent experiments. T-test for independent samples, \*\*,  $P = 0.005$ .

1405 S6G. RNA-FISH of the GFP reporter mRNA (teal) from Fig. 5E in HeLa cells coexpressing  
1406 MCP-mCherry-SEC61B (magenta) to visualize colocalization between the mRNA and the rough  
1407 ER membrane. Representative confocal images are shown. Scale bar, 5  $\mu\text{m}$ .

1408 S6H. Line profiles of the fluorescence intensities of the arrows from (G).

1409 S6I. Quantification of the experiment from (G). Two line profiles were generated for each cell.  
1410 The Pearson's correlation coefficients between the reporter mRNA and the ER were  
1411 determined. For MCP,  $N = 26$  cells were analyzed, for MCP-SEC61B,  $N = 26$  cells were  
1412 analyzed. The horizontal line denotes the median and the error bars denote the 25<sup>th</sup> and 75<sup>th</sup>  
1413 percentiles. Mann-Whitney test, \*\*\*\*,  $P < 0.0001$ .

1414 S6J. Schematic of a second GFP-tagged mRNA reporter that investigates the influence of  
1415 subcellular mRNA localization on protein expression. Fusion of MCP to TRAP $\alpha$  localizes the  
1416 GFP reporter mRNA to the ER membrane, whereas MCP alone localizes it to the cytosol.

1417 S6K. Confocal live cell imaging of HeLa cells expressing mC-tagged TRAP $\alpha$ -MCP. Scale bar, 5  
1418  $\mu\text{m}$ .

1419 S6L. GFP protein expression of the reporter mRNAs from (J) coexpressing the indicated MCP-  
1420 fusion constructs in HeLa cells measured by FACS. Representative histograms are shown. The  
1421 histograms on the left indicate GFP-negative cell populations.

1422 S6M. Quantification of the experiment from (L). Shown is the mean  $\pm$  std of four independent  
1423 experiments. T-test for independent samples, \*\*\*\*,  $P < 0.0001$ .

1424

1425 **Figure S7. Redirecting mRNA localization from the cytosol to the rough ER overcomes**  
1426 **the repressive effect of a bound RBP.**

1427 S7A. Confocal live cell imaging of HeLa cells expressing the indicated constructs. Shown are  
1428 representative images with TGs or cytosolic TIS11B. mC, mCherry. Scale bar, 5  $\mu\text{m}$ .

1429 S7B. Quantification from (A). The fraction of HeLa cells with TGs is shown after transfection of  
1430 the indicated TIS11B fusion constructs.  $N = 165$  cells were analyzed for mCherry-TIS11B and  $N$   
1431 = 198 cells were analyzed for MCP-mCherry-TIS11B. MCP-mCherry-TIS11B largely prevents  
1432 TG formation.

1433 S7C. Schematic of a second TIS11B-bound mRNA reporter that allows investigation of mRNA  
1434 localization-dependent GFP expression. The coding region of the reporter is provided by BIRC3,  
1435 followed by MS2 binding sites. Tethering of MCP or TIS11B localizes the mRNA reporter to the  
1436 cytosol, whereas the MCP-TIS11B-SEC61B fusion localizes the mRNA reporter to the rough  
1437 ER.  
1438 S7D. GFP protein expression of the reporter mRNA from (C) in HeLa cells, coexpressing the  
1439 indicated MCP-fusion constructs, measured by FACS. Representative histograms are shown.  
1440 The histograms on the left indicate GFP-negative cell populations.  
1441 S7E. Quantification of the experiment from (D). Shown is the mean ± std of four independent  
1442 experiments. T-test for independent samples, \*\*\*\*,  $P < 0.0001$ , MCP vs TIS11B-SEC61B:  $P =$   
1443 0.058; NS).

1444

1445

## 1446 References

1447

- 1448 1. Huttelmaier, S., Zenklusen, D., Lederer, M., Dictenberg, J., Lorenz, M., Meng, X.,  
1449 Bassell, G.J., Condeelis, J., and Singer, R.H. (2005). Spatial regulation of beta-actin  
1450 translation by Src-dependent phosphorylation of ZBP1. *Nature* 438, 512-515.  
10.1038/nature04115.
- 1451 2. Lecuyer, E., Yoshida, H., Parthasarathy, N., Alm, C., Babak, T., Cerovina, T., Hughes,  
1452 T.R., Tomancak, P., and Krause, H.M. (2007). Global analysis of mRNA localization  
1453 reveals a prominent role in organizing cellular architecture and function. *Cell* 131, 174-  
1454 187. S0092-8674(07)01022-7 [pii]10.1016/j.cell.2007.08.003.
- 1455 3. Moor, A.E., Golan, M., Massasa, E.E., Lemze, D., Weizman, T., Shenhav, R., Baydatch,  
1456 S., Mizrahi, O., Winkler, R., Golani, O., et al. (2017). Global mRNA polarization regulates  
1457 translation efficiency in the intestinal epithelium. *Science* 357, 1299-1303.  
10.1126/science.aan2399.
- 1458 4. Tushev, G., Glock, C., Heumuller, M., Biever, A., Jovanovic, M., and Schuman, E.M.  
1459 (2018). Alternative 3' UTRs Modify the Localization, Regulatory Potential, Stability, and  
1460 Plasticity of mRNAs in Neuronal Compartments. *Neuron* 98, 495-511 e496.  
10.1016/j.neuron.2018.03.030.
- 1461 5. Glock, C., Biever, A., Tushev, G., Nassim-Assir, B., Kao, A., Bartnik, I., Tom Dieck, S.,  
1462 and Schuman, E.M. (2021). The translatome of neuronal cell bodies, dendrites, and  
1463 axons. *Proc Natl Acad Sci U S A* 118. 10.1073/pnas.2113929118.
- 1464 6. Moretti, F., Rolando, C., Winker, M., Ivanek, R., Rodriguez, J., Von Kriegsheim, A.,  
1465 Taylor, V., Bustin, M., and Pertz, O. (2015). Growth Cone Localization of the mRNA  
1466 Encoding the Chromatin Regulator HMGN5 Modulates Neurite Outgrowth. *Mol Cell Biol*  
1467 35, 2035-2050. 10.1128/MCB.00133-15.
- 1468 7. Buxbaum, A.R., Haimovich, G., and Singer, R.H. (2015). In the right place at the right  
1469 time: visualizing and understanding mRNA localization. *Nature reviews. Molecular cell*  
1470 biology
- 1471 16, 95-109. 10.1038/nrm3918.
- 1472 8. Biever, A., Donlin-Asp, P.G., and Schuman, E.M. (2019). Local translation in neuronal  
1473 processes. *Current opinion in neurobiology* 57, 141-148. 10.1016/j.conb.2019.02.008.
- 1474 9. Reid, D.W., and Nicchitta, C.V. (2012). Primary role for endoplasmic reticulum-bound  
1475 ribosomes in cellular translation identified by ribosome profiling. *J Biol Chem* 287, 5518-  
1476 5527. 10.1074/jbc.M111.312280.

1477

1478

- 1479 10. Jan, C.H., Williams, C.C., and Weissman, J.S. (2014). Principles of ER cotranslational  
1480 translocation revealed by proximity-specific ribosome profiling. *Science* 346, 1257521.  
1481 10.1126/science.1257521.
- 1482 11. Fazal, F.M., Han, S., Parker, K.R., Kaewsapsak, P., Xu, J., Boettiger, A.N., Chang, H.Y.,  
1483 and Ting, A.Y. (2019). Atlas of Subcellular RNA Localization Revealed by APEX-Seq.  
1484 *Cell* 178, 473-490.e426. 10.1016/j.cell.2019.05.027.
- 1485 12. Qin, W., Myers, S.A., Carey, D.K., Carr, S.A., and Ting, A.Y. (2021). Spatiotemporally-  
1486 resolved mapping of RNA binding proteins via functional proximity labeling reveals a  
1487 mitochondrial mRNA anchor promoting stress recovery. *Nature communications* 12,  
1488 4980. 10.1038/s41467-021-25259-2.
- 1489 13. Xia, C., Fan, J., Emanuel, G., Hao, J., and Zhuang, X. (2019). Spatial transcriptome  
1490 profiling by MERFISH reveals subcellular RNA compartmentalization and cell cycle-  
1491 dependent gene expression. *Proc Natl Acad Sci U S A* 116, 19490-19499.  
1492 10.1073/pnas.1912459116.
- 1493 14. Banani, S.F., Lee, H.O., Hyman, A.A., and Rosen, M.K. (2017). Biomolecular  
1494 condensates: organizers of cellular biochemistry. *Nature reviews. Molecular cell biology*  
1495 18, 285-298. 10.1038/nrm.2017.7.
- 1496 15. Shin, Y., and Brangwynne, C.P. (2017). Liquid phase condensation in cell physiology  
1497 and disease. *Science* 357. 10.1126/science.aaf4382.
- 1498 16. Ma, W., and Mayr, C. (2018). A Membraneless Organelle Associated with the  
1499 Endoplasmic Reticulum Enables 3'UTR-Mediated Protein-Protein Interactions. *Cell* 175,  
1500 1492-1506 e1419. 10.1016/j.cell.2018.10.007.
- 1501 17. Peeples, W., and Rosen, M.K. (2021). Mechanistic dissection of increased enzymatic  
1502 rate in a phase-separated compartment. *Nature chemical biology* 17, 693-702.  
1503 10.1038/s41589-021-00801-x.
- 1504 18. Gasparski, A.N., Mason, D.E., Moissoglu, K., and Mili, S. (2022). Regulation and  
1505 outcomes of localized RNA translation. *Wiley interdisciplinary reviews. RNA* 13, e1721.  
1506 10.1002/wrna.1721.
- 1507 19. Luo, Y., Pratihar, S., Horste, E.H., Mitschka, S., Mey, A.S.J.S., Al-Hashimi, H.M., and  
1508 Mayr, C. (2023). mRNA interactions with disordered regions control protein activity.  
1509 *bioRxiv*, 2023.2002.2018.529068. 10.1101/2023.02.18.529068.
- 1510 20. Gasparski, A.N., Moissoglu, K., Pallikkuth, S., Meydan, S., Guydosh, N.R., and Mili, S.  
1511 (2023). mRNA Location and Translation Rate Determine Protein Targeting to Dual  
1512 Destinations. *bioRxiv*, 2023.2004.2024.538105. 10.1101/2023.04.24.538105.
- 1513 21. Ma, W., Zhen, G., Xie, W., and Mayr, C. (2021). In vivo reconstitution finds multivalent  
1514 RNA-RNA interactions as drivers of mesh-like condensates. *eLife* 10.  
1515 10.7554/eLife.64252.
- 1516 22. Han, X., Zhou, Z., Fei, L., Sun, H., Wang, R., Chen, Y., Chen, H., Wang, J., Tang, H.,  
1517 Ge, W., et al. (2020). Construction of a human cell landscape at single-cell level. *Nature*  
1518 581, 303-309. 10.1038/s41586-020-2157-4.
- 1519 23. Hubstenberger, A., Courel, M., Benard, M., Souquere, S., Ernoult-Lange, M., Chouaib,  
1520 R., Yi, Z., Morlot, J.B., Munier, A., Fradet, M., et al. (2017). P-Body Purification Reveals  
1521 the Condensation of Repressed mRNA Regulons. *Mol Cell* 68, 144-157 e145.  
1522 10.1016/j.molcel.2017.09.003.
- 1523 24. Liu, X., and Fagotto, F. (2011). A method to separate nuclear, cytosolic, and membrane-  
1524 associated signaling molecules in cultured cells. *Science signaling* 4, pl2.  
1525 10.1126/scisignal.2002373.
- 1526 25. Villanueva, E., Smith, T., Pizzinga, M., Elzek, M., Queiroz, R.M.L., Harvey, R.F.,  
1527 Breckels, L.M., Crook, O.M., Monti, M., Dezi, V., et al. (2022). A system-wide  
1528 quantitative map of RNA and protein subcellular localisation dynamics. *bioRxiv*,  
1529 2022.2001.2024.477541. 10.1101/2022.01.24.477541.

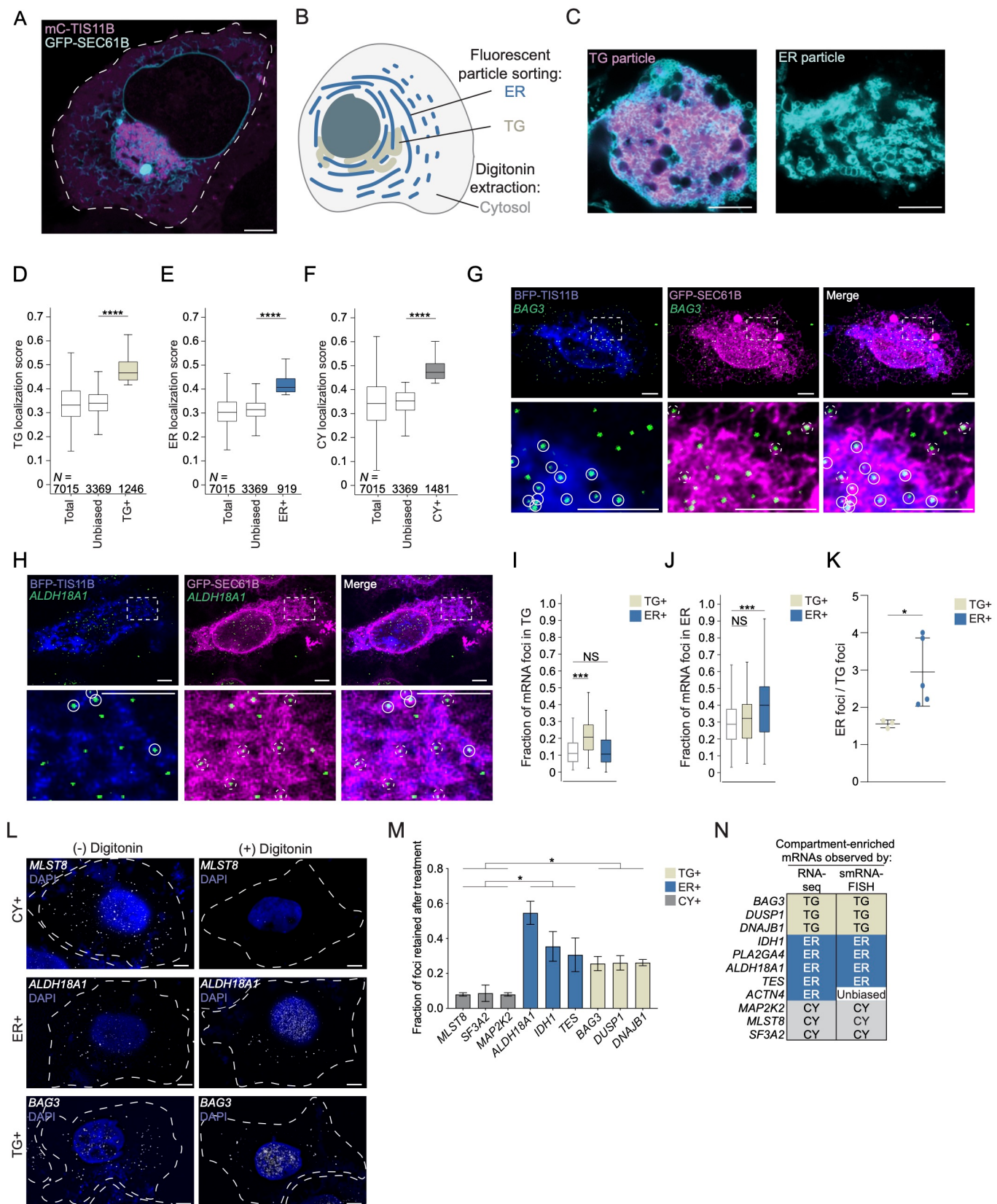
- 1530 26. Boraas, L., Hu, M., Thornton, L., Vejnar, C.E., Zhen, G., Giraldez, A.J., Mayr, C., Wang,  
1531 S., and Nicoli, S. (2021). Non-coding function for mRNAs in Focal Adhesion Architecture  
1532 and Mechanotransduction. *bioRxiv*, 2021.2010.2004.463097.  
1533 10.1101/2021.10.04.463097.
- 1534 27. Patel, R.K., West, J.D., Jiang, Y., Fogarty, E.A., and Grimson, A. (2020). Robust  
1535 partitioning of microRNA targets from downstream regulatory changes. *Nucleic Acids  
1536 Res* 48, 9724-9746. 10.1093/nar/gkaa687.
- 1537 28. Blumberg, A., Zhao, Y., Huang, Y.-F., Dukler, N., Rice, E.J., Chivu, A.G., Krumholz, K.,  
1538 Danko, C.G., and Siepel, A. (2021). Characterizing RNA stability genome-wide through  
1539 combined analysis of PRO-seq and RNA-seq data. *BMC biology* 19, 30.  
1540 10.1186/s12915-021-00949-x.
- 1541 29. Smalec, B.M., Ietswaart, R., Choquet, K., McShane, E., West, E.R., and Churchman,  
1542 L.S. (2022). Genome-wide quantification of RNA flow across subcellular compartments  
1543 reveals determinants of the mammalian transcript life cycle. *bioRxiv*,  
1544 2022.2008.2021.504696. 10.1101/2022.08.21.504696.
- 1545 30. Huang da, W., Sherman, B.T., and Lempicki, R.A. (2009). Systematic and integrative  
1546 analysis of large gene lists using DAVID bioinformatics resources. *Nature protocols* 4,  
1547 44-57. 10.1038/nprot.2008.211.
- 1548 31. Vaquerizas, J.M., Kummerfeld, S.K., Teichmann, S.A., and Luscombe, N.M. (2009). A  
1549 census of human transcription factors: function, expression and evolution. *Nature  
1550 reviews. Genetics* 10, 252-263. 10.1038/nrg2538.
- 1551 32. Yan, X., Hoek, T.A., Vale, R.D., and Tanenbaum, M.E. (2016). Dynamics of Translation  
1552 of Single mRNA Molecules In Vivo. *Cell* 165, 976-989. 10.1016/j.cell.2016.04.034.
- 1553 33. Küspert, M., Murakawa, Y., Schäffler, K., Vanselow, J.T., Wolf, E., Juranek, S.,  
1554 Schlosser, A., Landthaler, M., and Fischer, U. (2015). LARP4B is an AU-rich sequence  
1555 associated factor that promotes mRNA accumulation and translation. *Rna* 21, 1294-  
1556 1305. 10.1261/rna.051441.115.
- 1557 34. Zhao, W., Zhang, S., Zhu, Y., Xi, X., Bao, P., Ma, Z., Kapral, Thomas H., Chen, S.,  
1558 Zagrovic, B., Yang, Yucheng T., and Lu, Zhi J. (2021). POSTAR3: an updated platform  
1559 for exploring post-transcriptional regulation coordinated by RNA-binding proteins.  
1560 *Nucleic Acids Research* 50, D287-D294. 10.1093/nar/gkab702.
- 1561 35. Wang, Z., Kayikci, M., Briese, M., Zarnack, K., Luscombe, N.M., Rot, G., Zupan, B.,  
1562 Curk, T., and Ule, J. (2010). iCLIP predicts the dual splicing effects of TIA-RNA  
1563 interactions. *PLoS Biol* 8, e1000530. 10.1371/journal.pbio.1000530.
- 1564 36. Meyer, C., Garzia, A., Mazzola, M., Gerstberger, S., Molina, H., and Tuschl, T. (2018).  
1565 The TIA1 RNA-Binding Protein Family Regulates EIF2AK2-Mediated Stress Response  
1566 and Cell Cycle Progression. *Mol Cell* 69, 622-635 e626. 10.1016/j.molcel.2018.01.011.
- 1567 37. Bertrand, E., Chartrand, P., Schaefer, M., Shenoy, S.M., Singer, R.H., and Long, R.M.  
1568 (1998). Localization of ASH1 mRNA particles in living yeast. *Mol Cell* 2, 437-445.
- 1569 38. Berkovits, B.D., and Mayr, C. (2015). Alternative 3' UTRs act as scaffolds to regulate  
1570 membrane protein localization. *Nature* 522, 363-367. 10.1038/nature14321.
- 1571 39. Lee, S.H., and Mayr, C. (2019). Gain of Additional BIRC3 Protein Functions through 3'-  
1572 UTR-Mediated Protein Complex Formation. *Mol Cell* 74, 701-712 e709.  
1573 10.1016/j.molcel.2019.03.006.
- 1574 40. Voigt, F., Zhang, H., Cui, X.A., Triebold, D., Liu, A.X., Eglinger, J., Lee, E.S., Chao, J.A.,  
1575 and Palazzo, A.F. (2017). Single-Molecule Quantification of Translation-Dependent  
1576 Association of mRNAs with the Endoplasmic Reticulum. *Cell reports* 21, 3740-3753.  
1577 10.1016/j.celrep.2017.12.008.
- 1578 41. Stoecklin, G., Colombi, M., Raineri, I., Leuenberger, S., Mallaun, M., Schmidlin, M.,  
1579 Gross, B., Lu, M., Kitamura, T., and Moroni, C. (2002). Functional cloning of BRF1, a  
1580 regulator of ARE-dependent mRNA turnover. *EMBO J* 21, 4709-4718.

- 1581 42. Lykke-Andersen, J., and Wagner, E. (2005). Recruitment and activation of mRNA decay  
1582 enzymes by two ARE-mediated decay activation domains in the proteins TTP and BRF-  
1583 1. *Genes Dev* 19, 351-361. 10.1101/gad.1282305.
- 1584 43. Galloway, A., Saveliev, A., Lukasiak, S., Hodson, D.J., Bolland, D., Balmanno, K.,  
1585 Ahlfors, H., Monzon-Casanova, E., Mannurita, S.C., Bell, L.S., et al. (2016). RNA-  
1586 binding proteins ZFP36L1 and ZFP36L2 promote cell quiescence. *Science* 352, 453-  
1587 459. 10.1126/science.aad5978.
- 1588 44. He, P.C., Wei, J., Dou, X., Harada, B.T., Zhang, Z., Ge, R., Liu, C., Zhang, L.S., Yu, X.,  
1589 Wang, S., et al. (2023). Exon architecture controls mRNA m(6)A suppression and gene  
1590 expression. *Science* 379, 677-682. 10.1126/science.abj9090.
- 1591 45. Kedersha, N.L., Gupta, M., Li, W., Miller, I., and Anderson, P. (1999). RNA-binding  
1592 proteins TIA-1 and TIAR link the phosphorylation of eIF-2 alpha to the assembly of  
1593 mammalian stress granules. *The Journal of cell biology* 147, 1431-1442.  
1594 10.1083/jcb.147.7.1431.
- 1595 46. Gilks, N., Kedersha, N., Ayodele, M., Shen, L., Stoecklin, G., Dember, L.M., and  
1596 Anderson, P. (2004). Stress granule assembly is mediated by prion-like aggregation of  
1597 TIA-1. *Molecular biology of the cell* 15, 5383-5398. 10.1091/mbc.e04-08-0715.
- 1598 47. Mazan-Mamczarz, K., Lal, A., Martindale, J.L., Kawai, T., and Gorospe, M. (2006).  
1599 Translational repression by RNA-binding protein TIAR. *Mol Cell Biol* 26, 2716-2727.  
1600 10.1128/MCB.26.7.2716-2727.2006.
- 1601 48. Pacheco-Fiallos, B., Vorländer, M.K., Riabov-Bassat, D., Fin, L., O'Reilly, F.J., Ayala,  
1602 F.I., Schellhaas, U., Rappaport, J., and Plaschka, C. (2023). mRNA recognition and  
1603 packaging by the human transcription-export complex. *Nature* 616, 828-835.  
1604 10.1038/s41586-023-05904-0.
- 1605 49. Bonneau, F., Basquin, J., Steigenberger, B., Schäfer, T., Schäfer, I.B., and Conti, E.  
1606 (2023). Nuclear mRNPs are compact particles packaged with a network of proteins  
1607 promoting RNA-RNA interactions. *Genes Dev*. 10.1101/gad.350630.123.
- 1608 50. Hachet, O., and Ephrussi, A. (2004). Splicing of oskar RNA in the nucleus is coupled to  
1609 its cytoplasmic localization. *Nature* 428, 959-963. 10.1038/nature02521.
- 1610 51. Cheng, L.C., Zheng, D., Zhang, Q., Guvenek, A., Cheng, H., and Tian, B. (2021).  
1611 Alternative 3' UTRs play a widespread role in translation-independent mRNA association  
1612 with the endoplasmic reticulum. *Cell reports* 36, 109407. 10.1016/j.celrep.2021.109407.
- 1613 52. Cao, J., Wu, L., Zhang, S.M., Lu, M., Cheung, W.K., Cai, W., Gale, M., Xu, Q., and Yan,  
1614 Q. (2016). An easy and efficient inducible CRISPR/Cas9 platform with improved  
1615 specificity for multiple gene targeting. *Nucleic Acids Res* 44, e149. 10.1093/nar/gkw660.
- 1616 53. Sanjana, N.E., Shalem, O., and Zhang, F. (2014). Improved vectors and genome-wide  
1617 libraries for CRISPR screening. *Nat Methods* 11, 783-784. 10.1038/nmeth.3047.
- 1618 54. Thomas, J.D., Polaski, J.T., Feng, Q., De Neef, E.J., Hoppe, E.R., McSharry, M.V.,  
1619 Pangallo, J., Gabel, A.M., Belleville, A.E., Watson, J., et al. (2020). RNA isoform screens  
1620 uncover the essentiality and tumor-suppressor activity of ultraconserved poison exons.  
1621 *Nat Genet* 52, 84-94. 10.1038/s41588-019-0555-z.
- 1622 55. Zarnegar, B.J., Flynn, R.A., Shen, Y., Do, B.T., Chang, H.Y., and Khavari, P.A. (2016).  
1623 irCLIP platform for efficient characterization of protein-RNA interactions. *Nat Methods*  
1624 13, 489-492. 10.1038/nmeth.3840.
- 1625 56. Hu, M., Yang, B., Cheng, Y., Radda, J.S.D., Chen, Y., Liu, M., and Wang, S. (2020).  
1626 ProbeDealer is a convenient tool for designing probes for highly multiplexed  
1627 fluorescence in situ hybridization. *Sci Rep* 10, 22031. 10.1038/s41598-020-76439-x.
- 1628 57. Cui, X.A., Zhang, H., and Palazzo, A.F. (2012). p180 promotes the ribosome-  
1629 independent localization of a subset of mRNA to the endoplasmic reticulum. *PLoS Biol*  
1630 10, e1001336. 10.1371/journal.pbio.1001336.

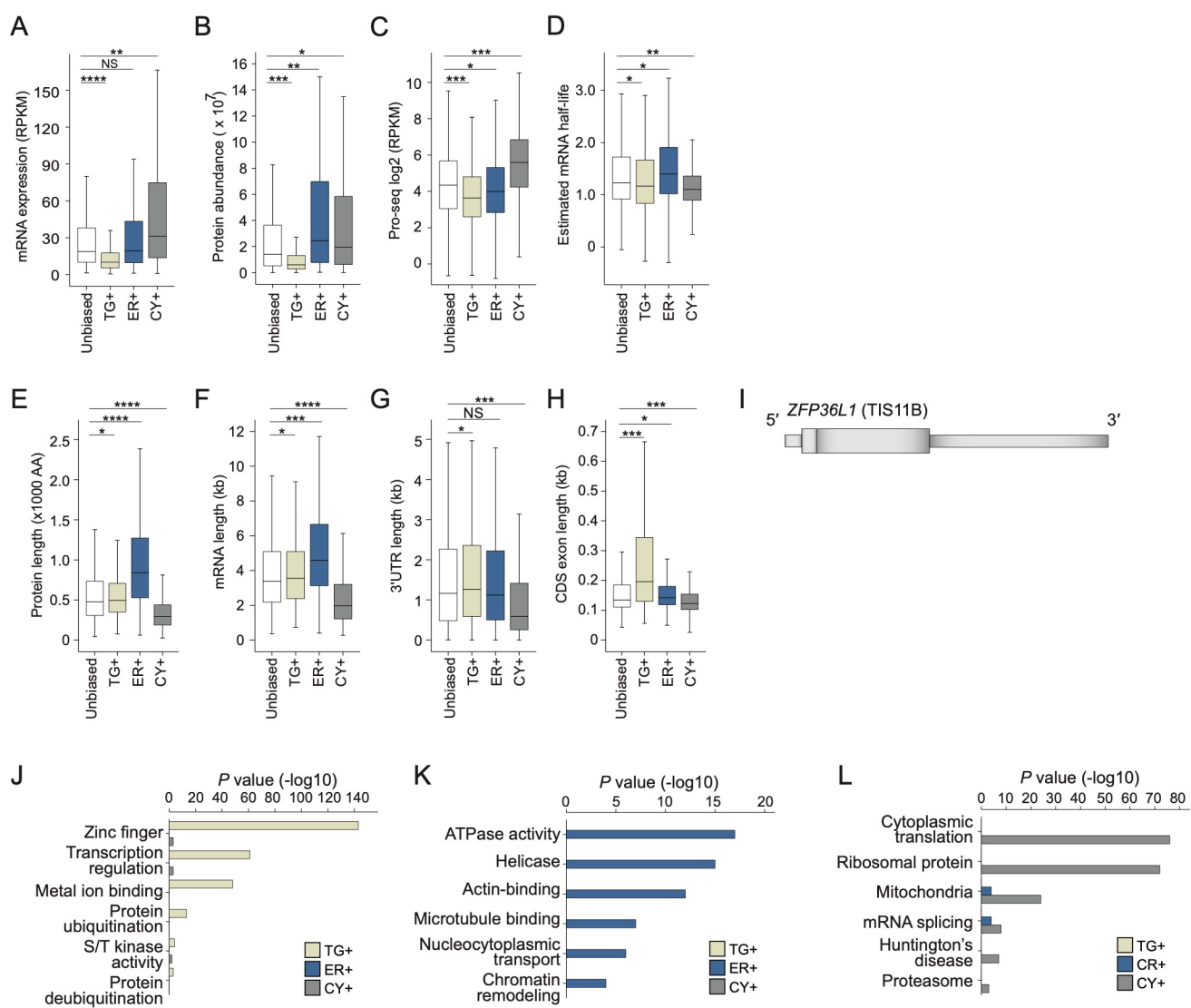
- 1631 58. Navarrete-Perea, J., Yu, Q., Gygi, S.P., and Paulo, J.A. (2018). Streamlined Tandem  
1632 Mass Tag (SL-TMT) Protocol: An Efficient Strategy for Quantitative (Phospho)proteome  
1633 Profiling Using Tandem Mass Tag-Synchronous Precursor Selection-MS3. *Journal of*  
1634 *proteome research* 17, 2226-2236. 10.1021/acs.jproteome.8b00217.  
1635 59. Rappaport, J., Mann, M., and Ishihama, Y. (2007). Protocol for micro-purification,  
1636 enrichment, pre-fractionation and storage of peptides for proteomics using StageTips.  
1637 *Nature protocols* 2, 1896-1906. 10.1038/nprot.2007.261.  
1638 60. Heinz, S., Benner, C., Spann, N., Bertolino, E., Lin, Y.C., Laslo, P., Cheng, J.X., Murre,  
1639 C., Singh, H., and Glass, C.K. (2010). Simple combinations of lineage-determining  
1640 transcription factors prime cis-regulatory elements required for macrophage and B cell  
1641 identities. *Mol Cell* 38, 576-589. 10.1016/j.molcel.2010.05.004.  
1642 61. Bolger, A.M., Lohse, M., and Usadel, B. (2014). Trimmomatic: a flexible trimmer for  
1643 Illumina sequence data. *Bioinformatics* 30, 2114-2120. 10.1093/bioinformatics/btu170.  
1644 62. Kim, D., Paggi, J.M., Park, C., Bennett, C., and Salzberg, S.L. (2019). Graph-based  
1645 genome alignment and genotyping with HISAT2 and HISAT-genotype. *Nat Biotechnol*  
1646 37, 907-915. 10.1038/s41587-019-0201-4.  
1647 63. Liao, Y., Smyth, G.K., and Shi, W. (2014). featureCounts: an efficient general purpose  
1648 program for assigning sequence reads to genomic features. *Bioinformatics* 30, 923-930.  
1649 10.1093/bioinformatics/btt656.  
1650 64. Morales, J., Pujar, S., Loveland, J.E., Astashyn, A., Bennett, R., Berry, A., Cox, E.,  
1651 Davidson, C., Ermolaeva, O., Farrell, C.M., et al. (2022). A joint NCBI and EMBL-EBI  
1652 transcript set for clinical genomics and research. *Nature* 604, 310-315. 10.1038/s41586-  
1653 022-04558-8.  
1654 65. Martin, M. (2011). Cutadapt removes adapter sequences from high-throughput  
1655 sequencing reads. 2011 17, 3. 10.14806/ej.17.1.200.  
1656 66. Dobin, A., Davis, C.A., Schlesinger, F., Drenkow, J., Zaleski, C., Jha, S., Batut, P.,  
1657 Chaisson, M., and Gingeras, T.R. (2013). STAR: ultrafast universal RNA-seq aligner.  
1658 *Bioinformatics* 29, 15-21. 10.1093/bioinformatics/bts635.  
1659 67. Frith, M.C., Valen, E., Krogh, A., Hayashizaki, Y., Carninci, P., and Sandelin, A. (2008).  
1660 A code for transcription initiation in mammalian genomes. *Genome Res* 18, 1-12.  
1661 10.1101/gr.6831208.

1662

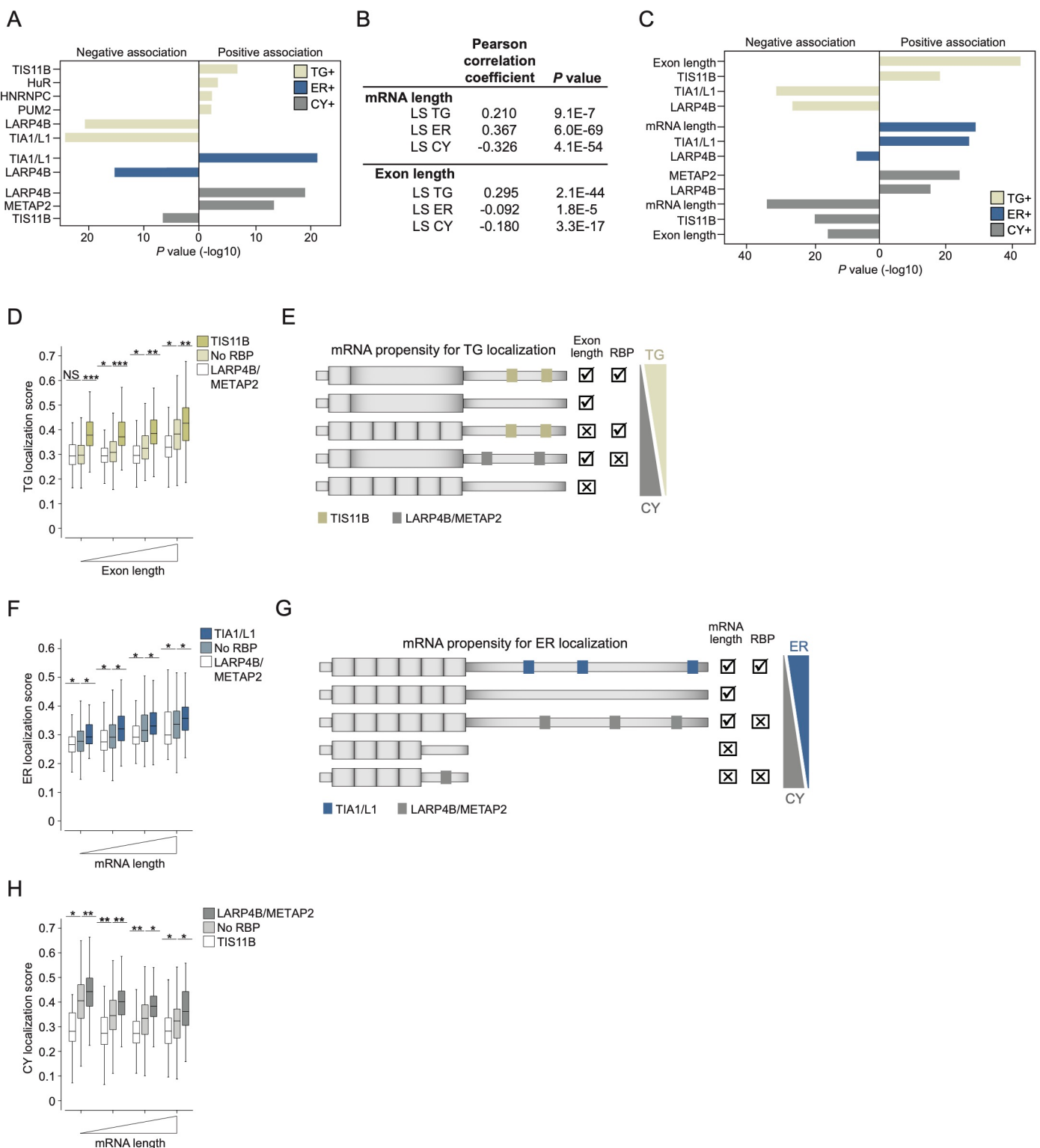
## Horste et al., Figure 1



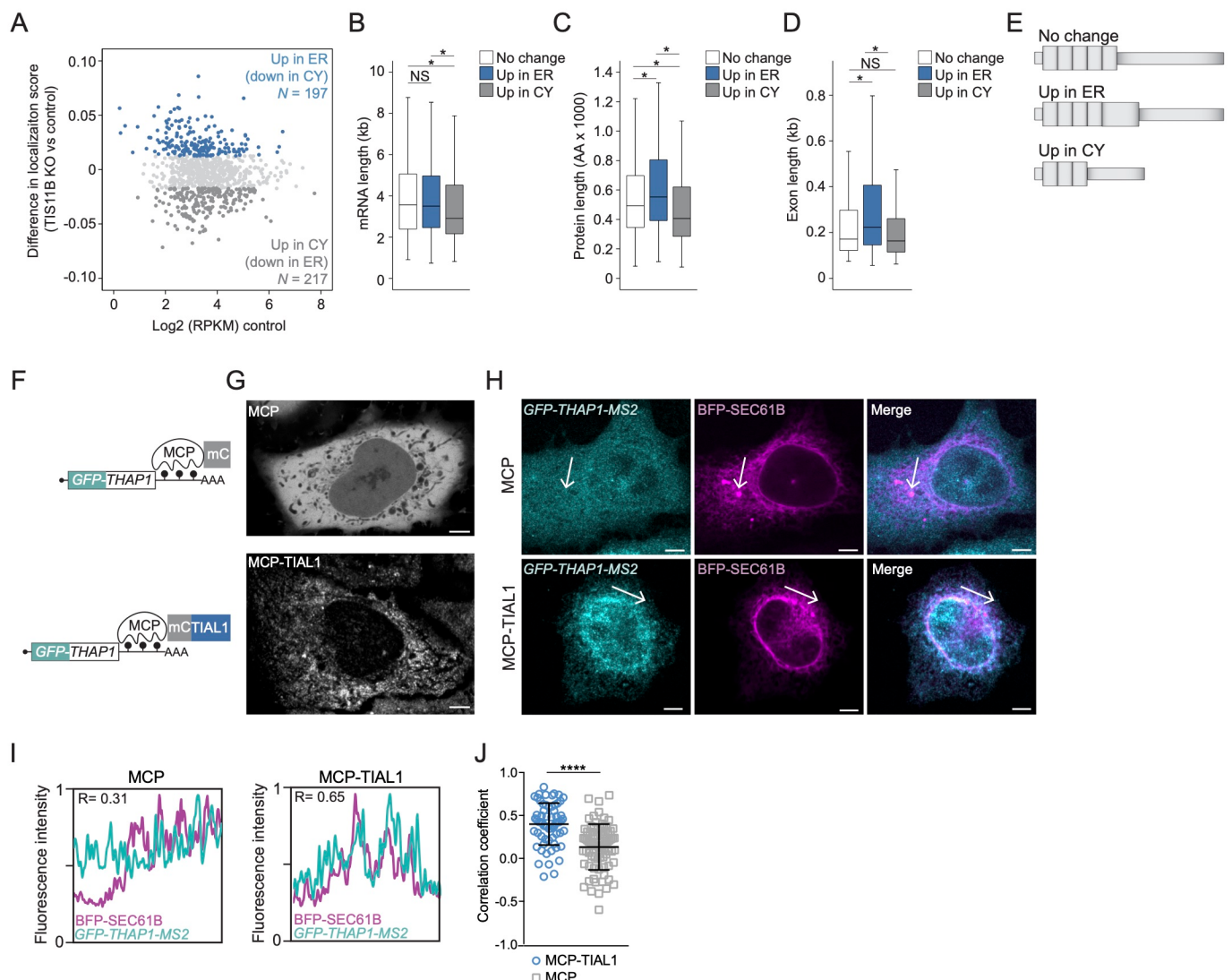
## Horste et al., Figure 2



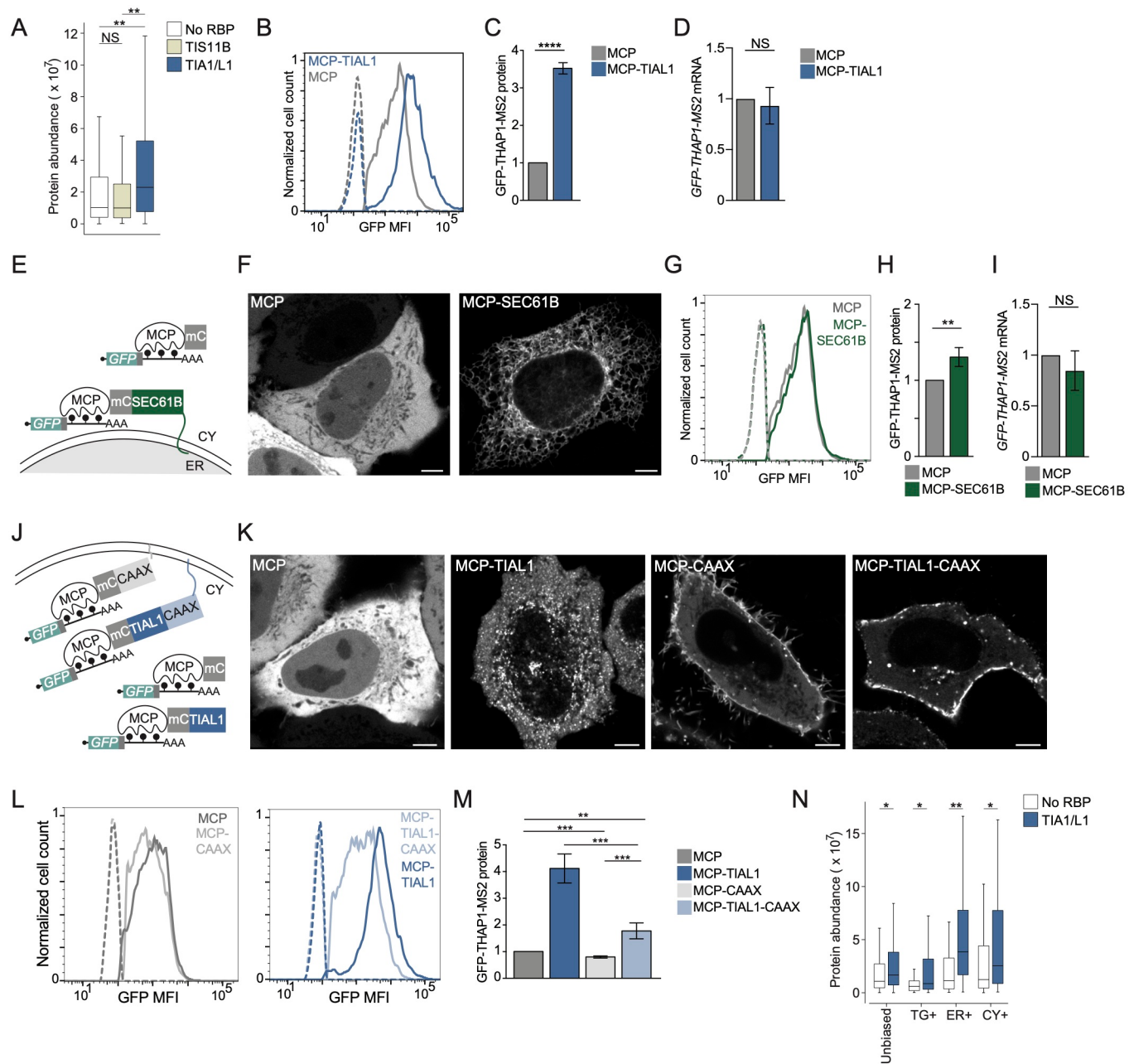
## Horste et al., Figure 3



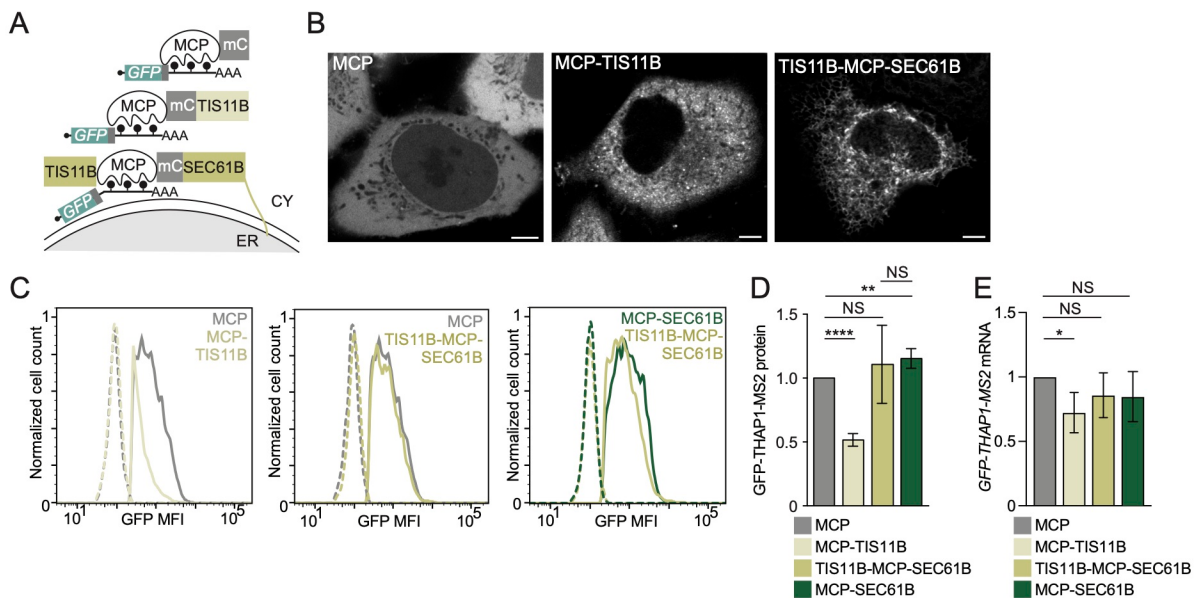
Horste et al., Figure 4



Horste et al., Figure 5



## Horste et al., Figure 6



Horste et al., Figure 7

